

Joint Estimation and Prediction of City-wide Delivery Demand: A Large Language Model Empowered Graph-based Learning Approach

Tong Nie^{a,b}, Junlin He^a, Yuwen Mei^b, Guoyang Qin^b, Guilong Li^a, Jian Sun^{b,*}, Wei Ma^{a,*}

^aDepartment of Civil and Environmental Engineering, The Hong Kong Polytechnic University, Hong Kong SAR, China

^bDepartment of Traffic Engineering, Tongji University, Shanghai, 201804, China

Abstract

The proliferation of e-commerce and urbanization has significantly intensified delivery operations in urban areas, boosting the volume and complexity of delivery demand. Data-driven predictive methods, especially those utilizing machine learning techniques, have emerged to handle these complexities in urban delivery demand management problems. One particularly pressing issue that has yet to be sufficiently addressed is the joint estimation and prediction of city-wide delivery demand, as well as the generalization of the model to new cities. To this end, we formulate this problem as a transferable graph-based spatiotemporal learning task. First, an individual-collective message-passing neural network model is formalized to capture the interaction between demand patterns of associated regions. Second, by exploiting recent advances in large language models (LLMs), we extract general geospatial knowledge encodings from the unstructured locational data using the embedding generated by LLMs. Last, to encourage the cross-city generalization of the model, we integrate the encoding into the demand predictor in a transferable way. Comprehensive empirical evaluation results on two real-world delivery datasets, including eight cities in China and the US, demonstrate that our model significantly outperforms state-of-the-art baselines in accuracy, efficiency, and transferability. **PyTorch implementation is available at: <https://github.com/tongnie/IMPEL>.**

Keywords: Urban logistics, Delivery demand, Demand estimation, Graph-based forecasting, Large language models

1. Introduction

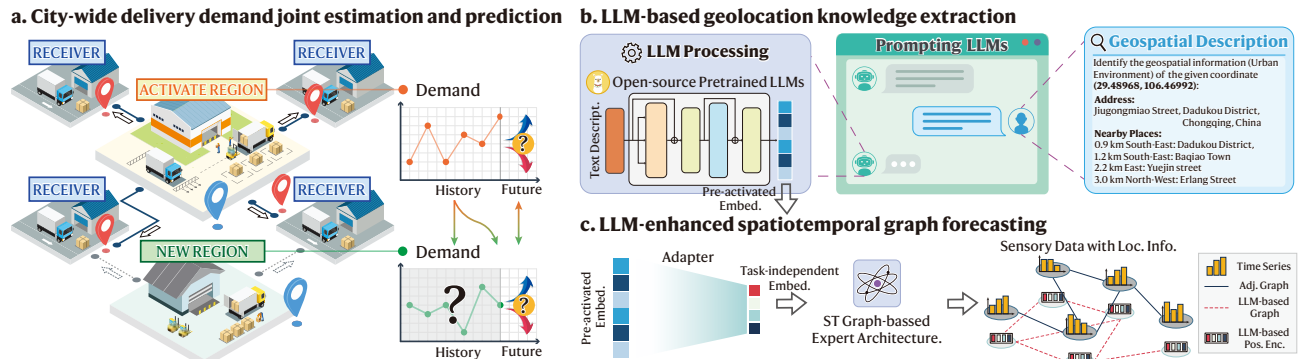


Figure 1: This paper studies the city-wide delivery demand joint estimation and prediction problem, with the objective of estimating the demands for new regions and predicting the future demands of both existing and developing regions. We address three key challenges: (1) modeling the interaction between demand patterns of correlated regions, (2) integrating unstructured geospatial information into the demand estimator/predictor, and (3) transferring the model to new cities without re-training. The solution is developed on the foundation of an LLM-based geolocation knowledge extraction module and an LLM-enhanced spatiotemporal graph forecasting architecture.

Driven by the rapid expansion of e-commerce and the concomitant increase in urban freight traffic, urban delivery demand management is of paramount significance due to its profound implications for various aspects of urban life, including urban mobility, environmental sustainability, and economic efficiency, emerging as a critical area of inquiry in transportation research. The increasing volume of deliveries in metropolitan areas has exacerbated traffic congestion, leading to longer travel times, higher fuel consumption, and greater greenhouse gas emissions (Yannis et al., 2006). As e-commerce continues to proliferate, the volume and complexity of delivery

*Corresponding authors.

Email addresses: sunjian@tongji.edu.cn (Jian Sun), wei.w.ma@polyu.edu.hk (Wei Ma)

operations in metropolitan areas have surged, necessitating more sophisticated and responsive management strategies. Thus, efficient management of delivery demand is crucial to alleviating these adverse effects, ensuring that delivery operations are both effective and sustainable (Black and Schreffler, 2010; Srinivas et al., 2022).

To efficiently manage delivery demand in urban logistics systems, a variety of specific tasks are studied to improve operational efficiency and sustainability, such as parking time optimization (Reed et al., 2024), route planning (He et al., 2022), system architecture design (Azcuy et al., 2021), and strategic design (Janjevic et al., 2019). These tasks rely heavily on the accurate and timely estimation (Muñozuri et al., 2012) and forecasting of the delivery demand (Hess et al., 2021; Nuzzolo and Comi, 2014). The significance of this issue is further underscored by several pressing challenges, including the high variability in demand patterns, the necessity for dynamic responsiveness in logistics operations, and precision in logistics planning. In this study, the term “*delivery demand*” is defined as the total number of pickup (or dropoff) delivery orders, including package and food orders, within a specified region of interest (ROI). Subsequently, the spatio-temporal evolution and distribution of city-wide demand patterns of all ROIs are examined.

Traditional approaches to demand forecasting and estimation have often been inadequate in addressing these variability and complexities due to their limited capacity for processing extensive demand datasets and reliance on static modeling approaches and simplistic assumptions. In response, there has been a substantial shift towards data-driven methods, particularly those facilitated by machine learning techniques and advanced data analytics, to offer a compelling advantage by providing enhanced predictive accuracy and real-time adaptability (Bajari et al., 2015). These advanced methods can analyze vast amounts of historical and real-time data, identifying demand patterns and trends that are not readily apparent through traditional methods, which are essential to address fluctuating demand for delivery and meet the evolving demands of modern cities.

Despite great advances that have been made in many real-world problems (Zeng et al., 2019; Li et al., 2021; Wu and Wu, 2019; Gao et al., 2021; Hess et al., 2021; Liang et al., 2023a), there are still some critical scenarios that remain underexplored and call for new modeling frameworks. Consider the case in which the demand values in operational regions are fully recorded in a region within a city. When new regions are planned for development in proximity to existing regions, managers endeavor to estimate and predict potential demands, as illustrated in Fig. 1. Furthermore, when a business seeks to expand to a new city where demand data are recorded over a relatively short period, it is essential to promptly evaluate the projected levels of future demand based on the limited records directly in order to ensure the adaptability of delivery strategies. In fact, operations in new regions have no historical data for reference. The model needs to exploit patterns from existing regions or transfer knowledge from the source cities to successfully predict expected demands.

To address this challenging issue, we break down the complexity into three key aspects as follows.

1. *How to model intricate interactions between the demand patterns of existing regions and newly developed ones.* It is anticipated that the construction of warehouses in new regions will influence the demand evolution of existing regions. Concurrently, the operational sphere of influence of preexisting warehouses will similarly exert a synergistic effect on the demand for new warehouses. This leads to an intricate interaction between the two items and is crucial for accurate demand estimation and prediction. Therefore, we assume that these interactive phenomena are composed of both region-specific patterns and region-wise dependencies, and propose to capture them using individual-collective graph representations.

2. *How to integrate adequate information to estimate unmeasured demands.* The delivery demand is influenced by many associated factors (Fancello et al., 2017; Fabusuyi et al., 2020). In particular, geospatial factors play an essential role in the emergence of last-mile delivery demand (Suguna et al., 2021). In this sense, collecting sufficient geolocational data becomes a prerequisite for an accurate estimation of city demand. However, collecting such data is nontrivial and requires a laborious process. In addition, different cities can have different data availability and source types. Specific geospatial data collected in a city may not be applicable to another city. An accessible data source is an urgent necessity. Fortunately, utilizing recent advances in large language models (LLMs), we can extract general geospatial knowledge from the unstructured locational data by exploiting the context reasoning ability of them. By integrating the transferable knowledge from LLMs into the spatial-temporal graph neural network (STGNN), our architecture can serve as a generalized demand estimator.

3. *How to guarantee the transferability of the model in new regions and cities.* Last, operators and managers often confront with the “cold-start” scenario in delivery operation. Models overfit to the training demand distribution may fail to transfer to new regions or cities without sufficient historical data for model re-training and fine-tuning. Therefore, the zero-shot transferability can facilitate the dynamic adjustment and adaptability of the strategic design. To achieve this, we first construct a functional graph that is generalizable to different cities relying on the encoding of LLMs. Then the backbone STGNN predictor is trained in an inductive manner with a joint reconstruction and forecasting task, ensuring its ability to generalize to new regions and cities in an end-to-end routine. Since the LLM-generated encoding requires no training and can be obtained offline, it enables prediction with varying numbers of new regions and cities at different scales. Based on this strategy, our model achieves three levels of transfer: (1) new regions without any demand records; (2) new cities with full current demand observations; and (3) new cities with partial current demands.

To evaluate the effectiveness of our method, we perform numerical experiments on two real-world delivery

order datasets in China and the US. The task includes both joint demand estimation and prediction and cross-city transfer. Extensive empirical results demonstrate that our model significantly outperforms state-of-the-art baselines in these challenging tasks. Comprehensive discussions are also provided to enhance interpretability. This paper involves the following contributions:

- We highlight the significance of location-based modeling in delivery demand joint estimation and prediction task and develop a data-driven scheme for extracting geolocation knowledge from LLMs;
- We present a method for integrating geolocation encoding into graph-based deep learning architectures. This approach allows for the modeling of both region-specific patterns and region-wide interactions in a unified graph representation, while simultaneously preserving the transferability across cities.
- Comprehensive evaluations using real-world urban delivery order datasets containing 8 cities from both China and the US demonstrate the effectiveness of our model. It is demonstrated that the performance gains in accuracy of the encoding are generic and it substantially improves cross-city transferability.

The rest of this paper is organized as follows. Section 2 reviews the existing literature on delivery demand management, spatiotemporal data modeling, and LLMs. Section 3 first provides the conceptualization and notation of the problem, then formulates the model framework and the solution. Section 5 evaluates the model in real-world delivery datasets. Section 6 provides a detailed discussion of the results and further studies. Section 7 concludes this work and provides future directions.

2. Related Work

In this section, we first review the related literature in urban delivery demand management and survey several representative tasks on this topic. Since the problem under study is related to the spatio-temporal data learning problem, we then briefly introduce recent advances in LLM-based spatio-temporal data modeling and advanced graph neural architectures.

2.1. Data-driven Urban Delivery Demand Management

The significant increase in urbanization and the advent of online commerce have elevated delivery demand management to a central concern in the realm of urban logistics systems. To evaluate the operational performance of the existing warehouse and delivery strategy, the records of pickup and delivery orders are collected and processed to develop analytical and data-centric models (Wen et al., 2024). These models are used to address real-world problems associated with logistics demand management, including last-mile delivery route planning (Zeng et al., 2019; Li et al., 2021), time of arrival estimation (Wu and Wu, 2019; Gao et al., 2021), route prediction (Wen et al., 2022), and demand prediction (Hess et al., 2021; Liang et al., 2023a; Nuzzolo and Comi, 2014). The majority of existing studies focus on package delivery or food delivery processes, utilizing private data within a singular logistics system. This increases the probability of drawing a conclusion that is biased towards a specific dataset. It is fortunate that an open-source dataset from industry (Wu et al., 2023) considerably facilitates data-driven applications. In addition to the above-studied problems, another fundamental task is to predict the demand level of newly developed regions. The issue is further complicated by the lack of historical data on the performance of new regions, as well as the impact of existing warehouses on the operations of new businesses.

2.2. Large Language Models for Spatial-Temporal Data

In recent years, large language models (LLMs) have made significant strides in the field of natural language processing. The advent of generative pre-trained transformers (GPTs) has ushered in a new era of modern machine learning, where large models have the potential to become a foundational architecture for a range of general language-related tasks. Representative LLMs include BERT (Devlin et al., 2018), Llama (Touvron et al., 2023), and Mistral (Jiang et al., 2023), and have been widely adopted for a wide range of disciplines. LLMs are distinguished for their excellent reasoning ability and in-context learning capability, which allows for few-shot or even zero-shot tasks (Brown et al., 2020; Kojima et al., 2022; Wei et al., 2021). A large number of studies have devoted to explore the potentials of LLMs to address fundamental problems in various areas. Most related to the problem studied, LLMs have demonstrated effectiveness in time series forecasting (Jin et al., 2023a; Garza and Mergenthaler-Canseco, 2023; Jia et al., 2024; Chang et al., 2023), spatial-temporal forecasting (Li et al., 2024; Jin et al., 2023b; Zhang et al., 2024b), and geospatial knowledge mining (Gurnee and Tegmark, 2023; Manvi et al., 2023, 2024; Tang et al., 2024). Moreover, LLMs have shown the potential to be integrated into transportation and mobility research, such as delivery route optimization (Liu et al., 2023; Qu et al., 2023), traffic data imputation (Zhang et al., 2024a), mobility demand prediction (Wang et al., 2023; Liang et al., 2024a; Gong et al., 2024), individual travel routine generation (Wang et al., 2024). Most of these methods adopt LLMs as backbone predictors either by transforming the input domain data to language tokens or fine-tuning LLMs with domain-specific instructions. In contrast to the aforementioned approach, we utilize LLMs as a generic geospatial encoder and enhance the downstream specialized model through the incorporation of LLM embedding, as opposed to employing them as the fundamental architectural component.

2.3. Spatial-Temporal Graph Neural Networks

Spatial-temporal graph neural networks (STGNNs) have become the leading approaches for graph-based spatiotemporal forecasting. STGNNs adopt sequential techniques such as recurrent neural networks (RNNs), temporal convolutional networks (TCNs) and self-attention to process temporal correlations. Spatial techniques such as graph convolution, node embedding, and message-passing neural networks are employed for exploiting spatial relational interactions. STGNNs have shown promising results using them for traffic flow forecasting, air quality prediction, and energy consumption management (Yu et al., 2018; Li et al., 2018; Wu et al., 2019a; Bai et al., 2020; Guo et al., 2019; Zheng et al., 2020; Shao et al., 2022c; Cini et al., 2022).

A recent trend has shifted the focus from the design of advanced architectures to the manipulation of data-specific patterns. Learnable node embedding is a representative solution (Shao et al., 2022a; Cini et al., 2023b; Nie et al., 2024c). Learnable embeddings are fed into modules of STGNNs and learned end-to-end with the forecasting tasks, enhancing the ability to identify node-specific patterns. Specifically, Shao et al. (2022b) used learnable embeddings for all nodes, time of day, and day of week stamps, allowing MLPs to achieve competitive performance in several datasets. Cini et al. (2023b) offered a systematic interpretation of node embedding as local effects and integrated it into a global-local architectural template. Fourier positional encoding was adopted in (Nie et al., 2024b) to enable canonical MLPs to capture high-frequency structures in traffic data.

Apart from the spatiotemporal forecasting tasks, STGNNs have also demonstrated effectiveness in other important tasks, such as the time series and spatiotemporal data imputation (Liang et al., 2022; Cini et al., 2021; Marasca et al., 2022; Nie et al., 2024a; Xue et al., 2024), spatiotemporal kriging (Wu et al., 2021a,c; Nie et al., 2024c; Zheng et al., 2023), and graph-based virtue sensing (De Felice et al., 2024). As we aim to forecast demand patterns for both operating areas with historical records and new areas without histories, the joint demand estimation and forecasting problem studied lies at the intersection of the two research venues, needing an integrated solution.

Similar to the delivery demand estimation task in urban logistics system, recent studies have elaborated advanced STGNNs to address mobility demand estimation problems in both micro and macro transportation systems (Xue et al., 2025). Representative works include bike sharing demand prediction (Liang et al., 2023c), dynamic flow distribution prediction in dockless e-scooter sharing system (He and Shin, 2020), trip generation for bike sharing platform planning (Liang et al., 2023b, 2024b), and mobility flow generation (Yao et al., 2020; Zhang et al., 2023; Liang et al., 2024c). Despite promising performance, these methods rely on handcrafted geospatial features with an arduous data collection process, such as POIs and distance metrics, to construct underlying graphs used as input to the model. Particularly, the transfer between observed locations and unobserved locations has been achieved in previous work by aggregating the representation learned for observed locations using a prescribed similarity metric (Liang et al., 2024b; Wei et al., 2024). However, this is sensitive to the choice of computation rules and the availability of supplementary data, making the model less generalizable across cities.

3. Model Formulation

In this section, we first formalized the demand joint estimation and prediction problem under the graph-based deep learning framework. Then techniques for extracting geospatial knowledge from LLMs are introduced. Finally, we formulate the model architecture and integrate all elements into an end-to-end inductive training scheme. The overview of our method is shown in Fig. 2. For brevity, we name our model: Inductive Message-Passing Neural Network with Encoding from LLMs (IMPEL).

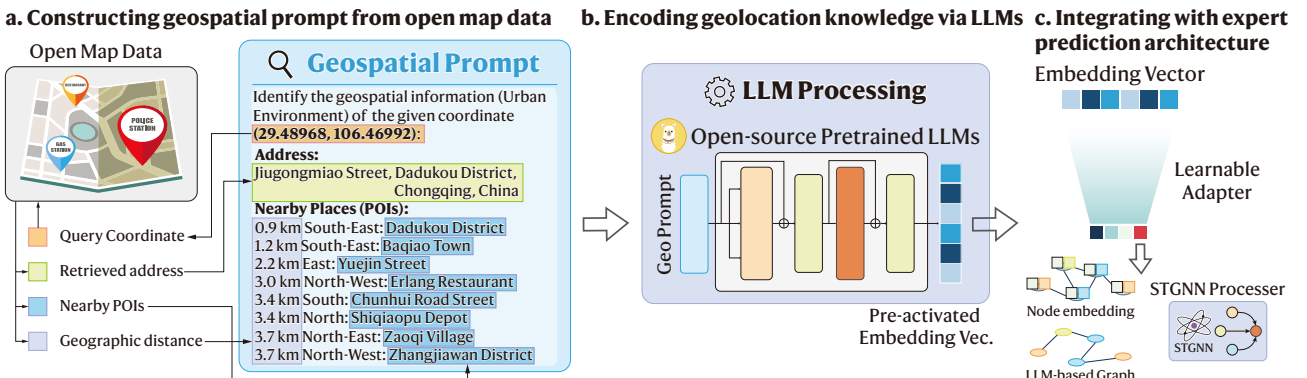


Figure 2: Overview of the methodology. We query LLMs using a prompt containing a basic geolocation description of the target region retrieved from OpenStreetMap. Then, the pre-activation embedding is extracted from the pre-trained LLM and fed into the downstream STGNN. The STGNN processes the vector in both node embedding and graph construction, enhancing transferability and accuracy.

3.1. Problem Conceptualization and Formulation

This paper processes the package and food delivery order datasets. These data contain the information associated with each order such as the pickup time τ_i and location $v_i = (x, y)_i$. By matching the location of each

pickup to the region of interests (ROIs) on the map and aggregating the total number of pickups to a specific time window, a dynamic demand matrix $\mathbf{X} \in \mathbb{R}^{N \times T}$ can be obtained:

$$x_t^n = \sum_i d_{n,t}^i, \quad d_{n,t}^i = \begin{cases} 1, & \text{if } \tau_i \in I_t \cap (x, y)_i \in R_n \\ 0, & \text{else} \end{cases}, \quad \forall n \in \{1, 2, \dots, N\}, t \in \{1, 2, \dots, T\}, \quad (1)$$

where R_n and I_t are the n -th ROI and t -th time interval. This definition can be readily extended to the multivariate case $\mathbf{x}_t^n \in \mathbb{R}^{d_x}$ that each region has d_x -dimensional observations, such as the demand of different products. Given regions $\{R_n\}_{n=1}^{N_o}$ where operations are already underway, managers expect to take advantage of its historical demand records to predict future demand values, as well as the estimated demand values for newly commissioned warehouses in regions $\{\bar{R}_n\}_{n=1}^{N_u}$. In addition, each region R_n (\bar{R}_n) is associated with a spatial location. We use the central point to represent the coordinate $\{\mathbf{v}_n\}_{n=1}^{\bar{N}}$ of each region with $\bar{N} = N_o + N_u$ and assume that all coordinates are available.

Then, given regions with available observations $\{\mathbf{X}_{\{1, \dots, T\}}^n\}_{n=1}^{N_o} \in \mathbb{R}^{T \times D}$ and coordinates $\{\mathbf{v}_n\}_{n=1}^{\bar{N}}$, for the next time horizon with length T' , the joint objective is to estimate a posterior probability:

$$p(\underbrace{\{\bar{\mathbf{X}}_{\{1, \dots, T\}}^n\}_{n=1}^{N_u}}_{\text{unobserved demand}}, \underbrace{\{\mathbf{X}_{t+T}^n\}_{n=1}^{\bar{N}}}_{\text{future demand}} | \underbrace{\{\mathbf{X}_{\{1, \dots, T\}}^n\}_{n=1}^{N_o}}_{\text{observed demand}}, \{\mathbf{v}_n\}_{n=1}^{\bar{N}}), \quad \forall t \in [1, T'], \quad (2)$$

where the unobserved historical demand is estimated and future demands for all regions are predicted. The standard demand time series forecasting task exploits rich historical patterns, and the demand estimation task emphasizes the relations between spatial units. The problem studied lies in the junction of the two. In contrast to previous work on demand estimation, we also advocate for the *transferability* of the model between different regions and cities, which is of high practical significance and yet to be fully explored.

As stated above, for new regions, both the historical and future values need to be estimated. For existing regions, the future values are based on both their historical demands and the existence of new regions. To approximate Eq. 2, our solution is to learn a predictive model parameterized by θ :

$$\theta = \arg \max_{\theta} \mathbb{E}[p_{\theta}(\{\bar{\mathbf{X}}_{\{1, \dots, T\}}^n\}_{n=1}^{N_u}, \{\mathbf{X}_{t+T}^n\}_{n=1}^{\bar{N}} | \{\mathbf{X}_{\{1, \dots, T\}}^n\}_{n=1}^{N_o}, \{\mathbf{v}_n\}_{n=1}^{\bar{N}})]. \quad (3)$$

To learn a parameterized function, we can exploit the relational dependencies existed in the training data as a reference. Three prominent types of dependencies that characterize this task are identified:

$$\begin{aligned} \mathcal{D}_{\text{intra}}^o &= \{\text{Corr}(\mathbf{x}_t^i, \mathbf{x}_t^j) | \forall R_i, R_j \in \{R_n\}_{n=1}^{N_o}\}, \\ \mathcal{D}_{\text{intra}}^u &= \{\text{Corr}(\bar{\mathbf{x}}_t^i, \bar{\mathbf{x}}_t^j) | \forall R_i, R_j \in \{\bar{R}_n\}_{n=1}^{N_u}\}, \\ \mathcal{D}_{\text{inter}}^{o,u} &= \{\text{Corr}(\mathbf{x}_t^i, \bar{\mathbf{x}}_t^j) | \forall R_i \in \{R_n\}_{n=1}^{N_o}, \forall R_j \in \{\bar{R}_n\}_{n=1}^{N_u}\}, \end{aligned} \quad (4)$$

which denote the intra-location and inter-location covariate sets, respectively. $\mathcal{D}_{\text{intra}}^o$ denotes the correlation between observed regions, which can be used to learn the relations between observations to predict future values. This is frequently discussed in the time series forecasting setting. $\mathcal{D}_{\text{intra}}^u$ includes the latent interactions between unobserved variables, which can be inferred from the message propagation of latent variables. Finally, learning in $\mathcal{D}_{\text{inter}}^{o,u}$ is the key to estimating unmeasured demands for new regions. In this case, a similarity metric is needed to describe relations between observed and unobserved locations. For example, proximity between coordinates $\{\mathbf{v}_n\}_{n=1}^{\bar{N}}$ can be used as a proxy in kriging models (Wu et al., 2021a). Instead, we model these dependencies using the functional similarity based on the knowledge extracted from LLMs. Meanwhile, we also associate each location with an encoding derived from LLMs, serving as an additional covariate for $\mathcal{D}_{\text{inter}}^{o,u}$.

The main notations used in this work are prescribed in Tab. 1.

3.2. Joint Demand Estimation and Prediction through Graph Models

We address the city-wide delivery demand joint estimation and prediction problem by formulating it as a graph-based spatiotemporal learning task. Based on the graph representation model, we then develop an inductive model training procedure to encourage transferability in new cities and regions.

3.2.1. Modeling Demand Patterns with Spatial-Temporal Graph Representations

We start by modeling the dynamic demand matrix as a multivariate time series set. Generally, each series i can have a d_x -dimensional record at each time step t , denoted by $\mathbf{x}_t^i \in \mathbb{R}^{d_x}$. Matrix $\mathbf{X}_{t:t+T}^i \in \mathbb{R}^{T \times d_x}$ denotes a single observed series within a given time window $\{t : t+T\}$. For simplicity, we also indicate $\mathbf{X}_t \in \mathbb{R}^{N_o \times d_x}$ as the collection of N_o sensors at time t . The N correlated demand series can be stacked as a tensor $\mathcal{X}_{t:t+T} = \{\mathbf{X}_{t:t+T}^i\}_{i=1}^{N_o} \in \mathbb{R}^{N_o \times d_x \times T}$. Some exogenous variables can also be collected, e.g., the date/time identifiers and events, and denoted by $\mathbf{u}_t \in \mathbb{R}^{d_u}$.

Table 1: Main notations used throughout the paper.

\mathbf{x}_t^i	The demand record of region i at time step t
$\mathbf{X}_{t:t+T}^i$	The demand series of region i within a period $t : t + T$
\mathbf{X}_t	The collection of N_t demand series at time stamp t
$\mathcal{X}_{t:t+T}$	All correlated demand series within a period $t : t + T$
\mathbf{A}	The proximity-based adjacency matrix of all regions
\mathbf{A}_t	The dynamic adjacency matrix of all regions at step t
\mathbf{V}	The coordinates of all regions
\mathbf{u}_t	The time-related exogenous variable
$\mathbf{m}_{t:t+T}^i$	An indicating variable to denote whether region i is observed within $t : t + T$
\mathcal{G}_t	The spatiotemporal graph comprised of several elements
W, H	The historical window size and forecasting horizon
$\ \mathbf{x}\ _p$	L^p norm of \mathbf{x}
ξ, σ, ψ, ρ	Nonlinear functions
$f(\mathbf{x}; \boldsymbol{\theta})$	A function of \mathbf{x} parametrized by $\boldsymbol{\theta}$. (Sometimes we write $f(\mathbf{x})$ and omit the argument $\boldsymbol{\theta}$ to lighten notation)
\mathcal{F}	A composition of functions, e.g., a graph neural network
\mathcal{L}	A deterministic loss function
$p(\cdot)$	A probability distribution over a continuous variable
$\mathbf{x} \sim p$	The variable \mathbf{x} has distribution P
$\mathbb{E}_{\mathbf{x} \sim p}[f(\mathbf{x})]$	Expectation of $f(\mathbf{x})$ with respect to $p(\mathbf{x})$

The generation of demand is determined by many interwoven factors. We assume that the system of demand generation constructs a time-invariant spatiotemporal stochastic process:

$$\mathbf{x}_\tau^i \sim p^i(\mathbf{x}_\tau^i | \mathcal{X}_{<\tau}, \mathbf{U}_{\leq \tau}), \forall i \in \{1, \dots, N_o\}, \forall \tau \in \{t : t + T\}, \quad (5)$$

where p is the conditional distribution, and $\mathbf{U}_{\leq \tau}$ is the stacked static features.

To instantiate Eq. 5, we assume the regularities of regional demand series follow a locality-aware graph polynomial vector autoregressive system (Isufi et al., 2019; Cini et al., 2023b):

$$\begin{aligned} \mathbf{H}_t &= \sum_{l=0}^L \sum_{p=1}^P \Psi_{p,l} \mathbf{S}^l [\mathbf{X}_{t-p} \| \mathbf{u}_{t-p}], \\ \mathbf{X}_t &= \mathbf{e} \odot \xi(\mathbf{H}_t) + \eta_t, \end{aligned} \quad (6)$$

where $\Psi \in \mathbb{R}^{P \times L}$ is the collection of model parameters, P is the total number of time lags, L is the total order of graph shifts, $\eta_t \sim \mathcal{N}(0, \sigma^2 \mathbb{I})$ is the Gaussian noise, ξ adds the nonlinearity, \mathbf{H}_t is the hidden state at step t , $\mathbf{e} \in \mathbb{R}^{N_o}$ simulates the region-specific patterns, \mathbf{S}^l is a graph shift operator derived from the graph Laplacian, e.g., $\mathbf{S} = \mathbf{D}^{-1/2}(\mathbf{I} + \mathbf{A})\mathbf{D}^{-1/2}$.

This graph-level spatiotemporal process delineates the evolution of all objects with regions as nodes. However, direct inference of parameters in this model is nontrivial, as it contains unknown latent variables. Therefore, we aim at learning a parameterized model $p_{\boldsymbol{\theta}}$ to approximate the unknown conditional probability function. Given a discrete historical window $\{t - W, \dots, t\}$, $\forall t$ we have:

$$p_{\boldsymbol{\theta}}(\mathbf{x}_{t+h}^i | \mathcal{X}_{t-W:t}, \mathbf{U}_{t-W:t+h}) \approx p^i(\mathbf{x}_{t+h}^i | \mathcal{X}_{<t}, \mathbf{U}_{\leq t+h}), \forall h \in [0, H], \forall i \in \{1, \dots, N_o\}. \quad (7)$$

Based on the assumption in Eq. 6, the multivariate demand time series is then abstracted as a *spatiotemporal graph*, with the relational relationships among the regions modeled as edges. The relational structures can be described by functional relationships between regions. Since the functional graph is nontrivial to obtain, we can use the adjacency graph to approximate the functional graph. Specifically, the adjacency graph can be calculated from the position of each region and their reciprocal physical proximity (Li et al., 2017), indicated by $\mathbf{A} \in \mathbb{R}^{N_o \times N_o}$. In a more general case, the number of ROIs can be time-varying, then the dynamic graph $\mathbf{A}_t \in \mathbb{R}^{N_o^t \times N_o^t}$ is considered. To model regional-level demand patterns, we assume that geographic information about each region is available and invariant with time. We use $\mathbf{V} \in \mathbb{R}^{N_o \times d_v}$ to represent the geolocation property of all ROIs, e.g., the spatial coordinates. Considering above elements, the observations can be organized as a sequence of spatiotemporal graphs $\{\mathcal{G}_t, \dots, \mathcal{G}_{t+T}\}$ with $\mathcal{G}_t = (\mathbf{X}_t, \mathbf{A}_t, \mathbf{V})$. Note that a basic assumption in this work is that the functional graph can capture the correlational or relational structures among the demand measurements, and the location of all ROIs are available and fixed at each time step.

After considering the multivariate dependencies among the demand series $\mathcal{X}_{t-W:t}$, the graph relational

structures can be encoded in the formulation as an inductive bias for the model architecture:

$$p_{\theta}(\mathbf{x}_{t+h}^i | \mathcal{G}_{t-W:t}, \mathbf{U}_{t-W:t+h}) \approx p^i(\mathbf{x}_{t+h}^i | \mathcal{X}_{<t}, \mathbf{U}_{\leq t+h}, \mathbf{V}), \forall h \in [1, H], \forall i \in \{1, \dots, N_o\}. \quad (8)$$

The above formulation only considers existing regions. After including the new regions, the demand joint estimation and forecasting problem in Eq. 2 can be rewritten using the graph representation:

$$\begin{aligned} \bar{\mathcal{G}}_{\tau} &= (\{\mathbf{x}_{\tau}^i\}_{i=1}^{N_o}, \bar{\mathbf{A}}_{\tau}, \bar{\mathbf{V}}), \\ \bar{\mathcal{X}}_{t-W:t}^u, \hat{\mathcal{X}}_{t:t+H} &= \mathcal{F}(\bar{\mathcal{G}}_{t-W:t}, \mathbf{U}_{t-W:t+H} | \theta) \text{ s.t. } \hat{\mathcal{X}}_{t:t+H} \approx \mathbb{E}_p[\mathcal{X}_{t:t+H}], \end{aligned} \quad (9)$$

where $\bar{\mathbf{A}}_{\tau} \in \mathbb{R}^{\bar{N}^t \times \bar{N}^t}$, $\bar{\mathbf{V}} \in \mathbb{R}^{\bar{N} \times d_v}$, $\hat{\mathcal{X}}_{t:t+H} = \{\mathbf{X}_{t:t+H}^i\}_{i=1}^{\bar{N}}$, $\hat{\mathcal{X}}_{t-W:t}^u = \{\bar{\mathbf{X}}_{t-W:t}^i\}_{i=1}^{N_u}$.

3.2.2. Parameterization by Space-then-Time Message Passing Network

After preparation of necessary components, we now formulate the expert backbone model, i.e., the parameterized of a spatial-temporal graph neural network (STGNN) \mathcal{F} instantiated by a message passing mechanism. Then we explain how this architectural template can be adapted to model both region-wise and city-wise demand dynamics.

Specifically, to model the time-varying representation of the delivery demand graph, we consider a spatiotemporal message passing neural network (STMPNN) with the ℓ -th layer formulated as follows:

$$\mathbf{x}_t^{i,\ell+1} = \psi^{\ell} \left(\mathbf{X}_{\leq t}^{i,\ell}, \text{AGGR}_{j \in \mathcal{N}(i)} \{ \rho^{\ell}(\mathbf{x}_{\leq t}^{i,\ell}, \mathbf{x}_{\leq t}^{j,\ell}, e_t^{i \leftarrow j}) \} \right), \quad (10)$$

where $\psi^{\ell} : \mathbb{R}^{d_{\ell}} \mapsto \mathbb{R}^{d_{\ell+1}}$ and $\rho^{\ell} : \mathbb{R}^{d_{\ell}} \times \mathbb{R}^{d_{\ell}} \mapsto \mathbb{R}^{d_{\ell}}$ are the message updating and message passing functions with possible nonlinearity. AGGR is a permutation invariant aggregation function, e.g., the summation. $\mathcal{N}(i)$ refers to neighbors of node i in the graph and $e_t^{i \leftarrow j}$ is the edge weight at time t .

To simplify the process, we assume the relational structure between nodes keeps static, and the above equation can be decoupled and instantiated as a *time-then-space* architecture (Gao and Ribeiro, 2022):

$$\mathbf{x}_t^{i,0} = \text{TEMPENC}(\mathbf{X}_{t-W:t}^{i,0}), \mathbf{x}_t^{i,\ell+1} = \psi^{\ell} \left(\mathbf{x}_t^{i,\ell}, \text{AGGR}_{j \in \mathcal{N}(i)} \{ \rho^{\ell}(\mathbf{x}_t^{i,\ell}, \mathbf{x}_t^{j,\ell}, e^{i \leftarrow j}) \} \right)_{\ell=0}^{L-1}, \quad (11)$$

where TEMPENC(\cdot) is a temporal processing module that correlates the point observation of each input sequence within the time window $\{t-W, \dots, t\}$. The time-then-space architectural template provides great efficiency benefits compared to alternating spatial and temporal processing. The TEMPENC(\cdot) aggregates temporal information at once; then the spatial (multivariate) dependencies are modeled by the spatial aggregation. Eq. 11 constitutes the backbone architecture of our model.

3.2.3. Collective-Individual Pattern Treatment Considering Transferability

\mathcal{F} defined in above section is trained to make predictions for a union set of all ROIs, without considering any region-specific demand patterns. This *collective* model that conditions on all multivariate demand series globally, explicitly capturing their correlations, and thus allowing transfer in new cities or regions in an inductive manner based on the training scheme in section 4.3. This makes global models suitable for cold-start scenarios, i.e., demand estimation for newly developed regions. However, it neglects the treatment of region-specific patterns. To consider individual effects and reformulate the global architecture in Eq. 11, we first revisit Eq. 7 following the terminology in Cini et al. (2023a). A global data generating model is given by:

$$p_{\theta}(\mathbf{x}_{t+h}^i | \mathbf{X}_{t-W:t}^i, \mathbf{U}_{t-W:t+h}, \mathbf{v}^i) \approx p^i(\mathbf{x}_{t+h}^i | \mathcal{X}_{<t}, \mathbf{U}_{\leq t+h}, \mathbf{V}), \forall h \in [1, H], \forall i \in \{1, \dots, \bar{N}\}, \quad (12)$$

where θ is the collection of global parameters that can be learned by optimizing the empirical loss over the entire demand series set $\mathcal{X}_{<t}$. Note that the demand variable $\mathcal{X}_{<t}$ contains latent variables, i.e., the demand of unmeasured regions. To further model the interaction among the demand patterns of different regions, i.e., the impact of local neighbor regions, we consider the multivariate extension:

$$p_{\theta}(\mathbf{x}_{t+h}^i | \bar{\mathcal{G}}_{t-W:t}, \mathbf{U}_{t-W:t+h}) \approx p(\mathcal{X}_{t+h} | \mathcal{X}_{<t}, \mathbf{U}_{\leq t+h}, \mathbf{V}), \forall h \in [1, H], \forall i \in \{1, \dots, \bar{N}\}, \quad (13)$$

where a joint distribution p of all nodes approximates the union of all individual distribution p^i and θ is shared across all regions. Indeed, if the global model is optimized over each series independently, e.g., the channel-independence (Nie et al., 2022), it approximates the joint distribution as:

$$p_{\theta}(\mathbf{x}_{t+h}^i | \bar{\mathcal{G}}_{t-W:t}, \mathbf{U}_{t-W:t+h}) \approx \prod_{i=1}^{\bar{N}} p^i(\mathbf{x}_{t+h}^i | \mathbf{X}_{<t}^i, \mathbf{U}_{\leq t+h}, \mathbf{v}^i). \quad (14)$$

Collective models have larger model capacities to process the relational information between regions. Since

collective models are learned by optimizing the expectation of the loss function over all regions, they may struggle to model region-specific patterns, i.e., p^i . However, as stated in Eq. 5, each demand series for a region can arise from different stochastic processes. The collective model needs an impractical large capacity to account for these variations (i.e., $\Pi_{i=1}^{\bar{N}} p^i$).

Instead, a node-level individual model used to approximate the data generating process is given by:

$$p_{\theta_i}^i(\mathbf{x}_{t+h}^i | \mathbf{X}_{t-W:t}^i, \mathbf{U}_{t-W:t+h}, \mathbf{v}^i) \approx p^i(\mathbf{x}_{t+h}^i | \mathcal{X}_{<t}, \mathbf{U}_{\leq t+h}, \mathbf{V}), \forall h \in [1, H], \forall i \in \{1, \dots, \bar{N}\}, \quad (15)$$

where θ_i is the i -th individual parameter fitted on the i -th region itself. In this case, each region can have individual model p^i and parameter θ_i . Individual models fit each specific demand series with a single model, thus overlooking the potential interaction among regions. Indeed, they are transductive that have difficulty in generalizing to new regions, i.e., the region set is *fixed* during all stages.

In practice, it is important to consider individual effects in the formulation of demand models. For instance, the demand pattern of each ROI is impacted not only by some shared patterns such as the holiday, promotional events, and seasonality, but also by their respective routines such as local events.

An ideal solution is to combine the strength of both collective and individual models (Grazzi et al., 2021; Cini et al., 2023b). Following (Cini et al., 2023b), the key step is to add specialized components to the global model, achieving a balance between the individual and collective modeling perspectives. Specifically, a typical kind of collective-individual hybrid model is given by:

$$p_{\theta, \{\phi_i\}}^i(\mathbf{x}_{t+h}^i | \mathbf{X}_{t-W:t}^i, \mathbf{U}_{t-W:t+h}, \mathbf{v}_{\phi_i}) \approx p^i(\mathbf{x}_{t+h}^i | \mathcal{X}_{<t}, \mathbf{U}_{\leq t+h}, \mathbf{V}), \forall i \in \{1, \dots, \bar{N}\}, \quad (16)$$

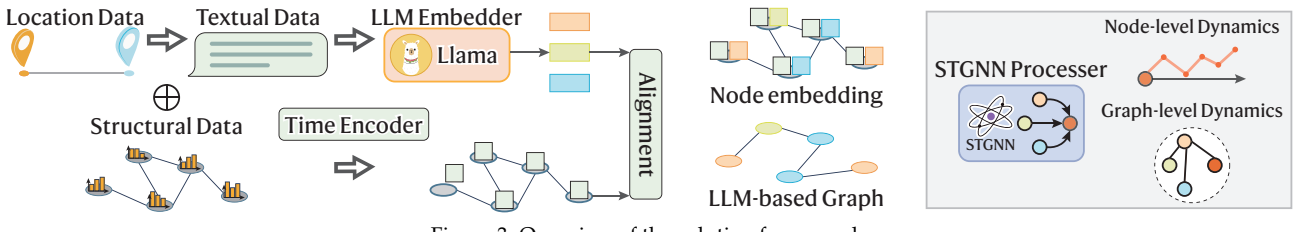
where $\{\phi_i\}_{i=1}^{\bar{N}}$ is the set of region-dependent parameters and we adopt it to parameterize each individual an index-based component, i.e., $\mathbf{v}_{\phi_i} \in \mathbb{R}^{d_{emb}}$. θ is the region-independent parameter shared globally. It is straightforward to find that the hypothesis class of all individual models in Eq. 15 is $\mathcal{H}_{\text{Ind}} = \{p(\cdot; \theta_i) | \theta_i \in \Theta, i = 1, \dots, \bar{N}\}$ where Θ is the parameter space. However, such a hypothesis class is too expensive and computationally infeasible for a large number of instances, e.g., a large dimension of regions. Instead, the reduced hypothesis class of collective-individual model is $\mathcal{H}_{\text{hybrid}} = \{p(\cdot; \theta, \phi_i) | \theta \in \Theta, \mathbf{v}_{\phi_i} \in \mathbb{R}^{d_{emb}}\}$, which is more feasible and efficient in optimization.

Finally, to implement Eq. 16 in a parameter-efficient way, Shao et al. (2022b) and Cini et al. (2023b) propose to assign each series a learnable embedding that can learn individual-dependent parameters during the training of the backbone architecture. Such a specialization provides flexibility for the globally shared model to condition representations at each series. Specifically, the predictor $\hat{\mathcal{X}}_{t:t+H} = \mathcal{F}(\bar{\mathcal{G}}_{t-W:t}, \mathbf{U}_{t-W:t+H} | \theta; \{\phi_i\}_{i=1}^{\bar{N}})$ with a shared architecture \mathcal{F} can be specialized by modulating the input and output layers using $\mathbf{v}_{\phi_i} \in \mathbb{R}^{d_{emb}}$ as follows.

$$\begin{aligned} \mathbf{h}_t^{i,(0)} &= \text{TEMPENC}(\mathbf{X}_{t-W:t}^{i,(0)}, \mathbf{U}_{t-W:t}, \mathbf{v}_{\phi_i}), \\ \mathbf{h}_t^{i,(\ell+1)} &= \psi^{(\ell)} \left(\mathbf{h}_t^{i,(\ell)}, \text{AGGR}_{j \in \mathcal{N}(i)} \{ \rho^{(\ell)}(\mathbf{h}_t^{i,(\ell)}, \mathbf{h}_t^{j,(\ell)}, e^{i \leftarrow j}) \} \right)_{\ell=0}^{L-1}, \\ \hat{\mathbf{x}}_{t+h}^i &= \text{OUTPUT}(\mathbf{h}_t^{i,(L)}, \mathbf{U}_{t:t+h}, \mathbf{v}_{\phi_i}), \forall h \in [1, H], \end{aligned} \quad (17)$$

where **OUTPUT** is usually implemented by a single MLP, and **TEMPENC**, ψ , ρ , and **OUTPUT** are shared by all regions. Instead of learning individual models for all regions in Eq. 15, the above scheme is more parameter-efficient and reduces the risk of overfitting. Before solving for this learning model, we need to address some queries: (1) The demand variable \mathcal{X} has latent variables, i.e., the demand of unmeasured regions; (2) Introducing region-specific parameters to the model that is not applicable to other regions sacrifices the transferability provided by pure collective models; (3) The characterization of geolocation information \mathbf{V} of all regions requires the integration of sufficient spatial data related with logistics demand, e.g., positions of interests.

4. Solution Framework



Although the above formulation can characterize variations and correlations of demand patterns at both levels, it is nontrivial to obtain such a parameterization to approximate Eq. 6. Specifically, the technical challenges for

the model solution are identified in three aspects. First, how to capture the node-level dynamics and graph-level interactions simultaneously and efficiently. Second, how to allow the model to transfer to new regions and new cities without retraining. Third, how to integrate essential geolocation knowledge into the model that is generalizable to different cities. To address these challenges, this section presents our solution framework that seamlessly aligns the embedding of LLMs with GNNs. This LLM-empowered graph-based learning solution provides a learnable and feasible parameterization to approximate Eq. 6. The solution framework is shown in Fig. 3.

4.1. Encoding Geospatial Knowledge from Large Language Models

Based on the above descriptions, this section introduces the integration of LLMs to encode geospatial knowledge and graph-based relational bias into the backbone architecture, i.e., the joint demand estimator and predictor. The role of LLM-based encoding is two-fold: (1) transferability region-specific embedding; (2) functional graph based on the similarity of geospatial encoding vector.

4.1.1. Location-based Geospatial Query

The sensory data such as demand series is highly associated with some location-dependent variables. However, collecting sufficient geospatial information, including points of interest, road network geometry, and buildings, can be a laborious and tedious process. This is especially difficult when different cities have different sources and availability of location data. Fortunately, recent advances in natural language processing provide an alternative paradigm for mining geospatial knowledge (Gurnee and Tegmark, 2023; Manvi et al., 2024). As LLMs have shown an impressive ability to reason about geospatial data (Manvi et al., 2023), it is expected to extract general location-based representations based on the intrinsic knowledge of LLMs.

To achieve this, we first construct a location-based query and organize a text prompt as input to LLMs. First, given the query coordinate $v = (x, y)$ of the target location, a public map service or database such as OpenStreetMap (OSM) (Haklay and Weber, 2008) is accessed and some general geolocation information is obtained, such as POIs and surrounding streets and buildings. Then a text message containing the basic location information extracted from the OSM is generated as a prompt and fed into LLMs, as shown in Fig. 2. LLMs are requested to identify and understand the geolocation information, relying on their ability to reason in context.

4.1.2. Prompt-based Geospatial Reasoning and Encoding Generation

Different from existing frameworks that adopt LLMs as the backbone forecasting backbone (Jin et al., 2023a), or directly generate geospatial message from the output (Manvi et al., 2023), we propose to adopt the pre-activated embedding from the output layer of a pre-trained LLM as the latent covariate, which is assumed to be geospatially encoded by the network processing. To extract the general geospatial encoding from LLMs that is applicable for downstream tasks, we use the linear probing technique (Alain and Bengio, 2016; Belinkov, 2022). Specifically, given the network activation of hidden states (before the last softmax function) $\mathbf{H}_{\text{LLM}} \in \mathbb{R}^{\bar{N} \times D_{\text{LLM}}}$ of LLMs, we can use a linear ridge regressor as the probe to fit the node embedding of each ROI:

$$\widehat{\mathbf{W}}_{\text{prob}} = \arg \min_{\mathbf{W}_{\text{prob}}} \|\mathbf{E} - \mathbf{H}_{\text{LLM}} \mathbf{W}_{\text{prob}}\|_F^2 + \lambda \|\mathbf{W}_{\text{prob}}\|_F^2 = (\mathbf{H}_{\text{LLM}}^\top \mathbf{H}_{\text{LLM}} + \lambda \mathbf{I})^{-1} \mathbf{H}_{\text{LLM}}^\top \mathbf{E}, \quad (18)$$

where $\mathbf{E} \in \mathbb{R}^{\bar{N} \times D_{\text{node}}}$ is the empirical node embedding derived from the training data and $\mathbf{W}_{\text{prob}} \in \mathbb{R}^{D_{\text{LLM}} \times D_{\text{node}}}$. Although \mathbf{E} can be obtained by learning from the training set or be elaborated by handcrafted rules. However, an ideal node embedding is nontrivial to design across multiple cities with different demand patterns. Thus, we integrate this process in the end-to-end learning of network parameters (refer to 4.2). Note that $\widehat{\mathbf{W}}_{\text{prob}}$ is used to align the task-independent embedding of LLMs with the node representation, making it generalizable for adapting to demand patterns across cities.

4.1.3. Functional Graph Construction with LLM Encoding

As discussed in section 3.2.1, the correlation and interaction between regions are described by a graph. Due to the absence of a precise metric to construct such a graph, physical proximity is generally adopted (Lei et al., 2022; Nie et al., 2023a). However, proximity in the Euclidean is inadequate to reflect the relationships of demand patterns in feature space. Fortunately, the inherent geospatial knowledge in the LLM-based encoding provides an abstract of the geolocation property of each region in the latent space. We can measure the similarity of these encodings and treat it as a more accurate surrogate of the functional similarity. To achieve this, the functional graph is learned end-to-end simultaneously with the main architecture:

$$\bar{\mathcal{X}}_{t-W:t}^u, \hat{\mathcal{X}}_{t:t+H} = \mathcal{F}(\bar{\mathcal{G}}_{t-W:t}, \mathbf{U}_{t-W:t+H}, \mathbf{A}_{\text{LLM}} | \boldsymbol{\theta}), \mathbf{A}_{\text{LLM}} \sim q_{\Phi}(\bar{\mathbf{A}} | \bar{\mathcal{X}}_{t-W:t}) \in \mathbb{R}^{\bar{N} \times \bar{N}}, \quad (19)$$

where θ, Φ are the base and the graph learning parameter respectively, \mathbf{A}_{LLM} is the LLM-based functional graph. To jointly learn the parameters over the training set, we solve the following problem:

$$\begin{aligned} \theta^*, \Phi^* &= \arg \min_{\theta, \Phi} \frac{1}{T_{\text{train}}} \sum_{t=1}^{T_{\text{train}}} \mathbb{E}_{\mathbf{A}_{\text{LLM}} \sim q_{\Phi}} [\|\mathcal{F}(\bar{\mathcal{G}}_{t-W:t}, \mathbf{U}_{t-W:t+H}, \mathbf{A}_{\text{LLM}} | \theta) - \mathbf{x}_{t+h}^i\|_2^2], \\ &= \arg \min_{\theta, \Phi} \frac{1}{T_{\text{train}}} \sum_{t=1}^{T_{\text{train}}} \frac{1}{NH} \sum_{i=1}^N \sum_{h=1}^H \|\mathcal{F}(\bar{\mathcal{G}}_{t-W:t}, \mathbf{U}_{t-W:t+H}, \mathbf{A}_{\text{LLM}} | \theta) - \mathbf{x}_{t+h}^i\|_2^2, \end{aligned} \quad (20)$$

where T_{train} is the total time steps of the training dataset. Eq. 20 is achieved in the forecasting loss in Eq. 32 and can be solved by typical gradient-based methods. The following paragraphs will elaborate the backbone architecture \mathcal{F} for processing the graph representation of the demand time series.

4.2. LLM-Enhanced Collective-Individual Graph-based Learning

Next, we demonstrate how the encoding from LLMs and the LLM-based functional graph can be integrated into the architectural template and elaborate the detailed choice of modular components.

4.2.1. Integration of Encodings from LLMs

Recall that applying region-specific parameters in the collective model can efficiently account for the effects that characterize individual treatments, thereby improving the predictive performance on the current task. However, this scheme also sacrifices the flexibility provided by pure collective models: it cannot perform inductive learning in a model-based manner, leading to a compromise in transferability. This is because the learned individual parameter cannot be applied to regions outside the training data. To compensate for this ideal property, we proposed resorting to generalizable embedding from LLMs. We suggest the integration of the LLM-based embedding in two ways.

First, since LLMs can encode comprehensive knowledge that humans can understand, we exploit this encoding as the co-variate of demand series and incorporate it in both the temporal encoder and message passing modules to serve as the local effects discussed in subsection 3.2.3:

$$\begin{aligned} \mathbf{v}_{\phi_i} &= \mathbf{H}_{\text{LLM}} \widehat{\mathbf{W}}_{\text{prob}}, \\ \widetilde{\mathbf{v}}_{\phi_i} &= \text{BATCHNORM}(\text{LEAKYRELU}(\mathbf{v}_{\phi_i})), \\ \mathbf{h}_t^{i,(0)} &= \text{TEMPENC}([\mathbf{X}_{t-W:t}^{i,(0)} \| \widetilde{\mathbf{v}}_{\phi_i}], \mathbf{U}_{t-W:t}), \\ \mathbf{h}_t^{i,(\ell+1)} &= \psi^{(\ell)} \left(\mathbf{h}_t^{i,(\ell)}, \text{AGGR}_{j \in \mathcal{N}_k(i)} \{ \rho^{(\ell)}([\mathbf{h}_t^{i,(\ell)} \| \widetilde{\mathbf{v}}_{\phi_i}], \mathbf{h}_t^{j,(\ell)}, e^{i \leftarrow j}) \} \right)_{\ell=0}^{L-1}, \end{aligned} \quad (21)$$

where $\mathbf{H}_{\text{LLM}}, \widehat{\mathbf{W}}_{\text{prob}}$ are introduced in Eq. 18, and $\widetilde{\mathbf{v}}_{\phi_i} \in \mathbb{R}^{D_{\text{node}}}$ is the LLM-based node embedding, BATCHNORM is used to reduce the variance of different encodings, and $[\cdot \| \cdot]$ is the concatenation.

Second, learning an appropriate graph in a data-dependent way (see Eq. 20) is not easy. To efficiently implement this scheme, we make \mathbf{A}_{LLM} implicitly conditions on $\bar{\mathcal{X}}_{t-W:t}$. Specifically, we first set a layerwise *adapter* $\mathbf{D} \in \mathbb{R}^{D_{\text{graph}}^{(\ell)} \times D_{\text{node}}}$ shared by all regions, to reduce the parameter space:

$$\mathbf{v}_{g,\phi_i} = \text{LEAKYRELU}(\mathbf{D}^{(\ell)} \mathbf{v}_{\phi_i}), \quad (22)$$

where $\Phi = \{\mathbf{D}^{(\ell)}\}_{\ell=0}^L$ is the parameter set for graph learning in Eq. 20. Then the LLM-based functional graph is simplified as an undirected graph as follows:

$$e^{i \leftarrow j} = \langle \mathbf{v}_{g,\phi_i}, \mathbf{v}_{g,\phi_j} \rangle, \quad \mathcal{E} = \{e^{i \leftarrow j} \mid \forall i, j \in 1, \dots, \bar{N}\}, \quad (23)$$

where $\langle \cdot \rangle$ is the vector inner product, \mathcal{E} is the set of fully-connected graph edges.

Intuitively, for regions without historical time series records, the LLM-based encoding provides an expressive latent variable to regress the target value. For regions with observations, both the data and the encoding contribute to the estimation and forecasting. The aggregation of the neighbor encoding and node value in the LLM-based functional graph enables the model to be inductive.

Remark. (Comparison with Learnable Region (Node) Embedding.) Note that both the learnable embedding (Shao et al., 2022a) and our LLM-based encoding for each region (node) can account for the region-specific patterns. However, the learnable embedding is fitted to the training data distribution with full observations available. When transfers to new regions without available observations for training or fine-tuning, the learnable embedding fails to adapt to new data. Instead, our LLM-based encoding is precomputed prior to model training and fixed throughout the learning process. This makes it generalizable across new regions and cities.

4.2.2. Implementation Details of Modular Computations

Finally, we explain the details of model implementations, particularly the instantiating of Eq. 11. **Temporal message-passing layers (TEMPENC)**:

$$\mathbf{h}_t^{i,\ell+1} = \psi^\ell \left(\mathbf{h}_t^{i,\ell}, \text{AGGR}_{\leq t} \rho^\ell(\mathbf{x}_t^{i,\ell}, \mathbf{X}_{\leq t}^{i,\ell}) \right). \quad (24)$$

In practice, recurrent neural networks (RNNs), temporal convolutional networks (TCN), and Transformers can be adopted for Eq. 24. As an alternative, MLP-based architectures such as TSMixers (Chen et al., 2023) have proven to be a more efficient and flexible choice. Specifically, we choose:

$$h_t^{i,\ell+1} = \sigma(\mathbf{W}_t^\ell [\mathbf{x}_t^{i,\ell} \| \mathbf{x}_{t-1}^{i,\ell} \| \dots \| \mathbf{x}_{t-W}^{i,\ell}] + \mathbf{b}_t^\ell). \quad (25)$$

Spatial message-passing layers: we instantiate it as anisotropic graph neural networks (GNNs) (Satorras et al., 2022), with a k -th-order extension. For each k -hop neighborhood, we have:

$$\begin{aligned} \text{Message Updating: } \mathbf{m}_t^{j \rightarrow i, \ell} &= \sigma(\mathbf{W}_m^\ell [\mathbf{h}_t^{i,\ell} \| \mathbf{h}_t^{j,\ell} \| e_t^{i \leftarrow j}] + \mathbf{b}_m^\ell), \\ \text{Edge Updating: } \alpha_t^{j \rightarrow i, \ell} &= \sigma(\mathbf{W}_e^\ell \mathbf{m}_t^{j \rightarrow i, \ell} + \mathbf{b}_e^\ell), \\ \text{Node Updating: } \mathbf{h}_t^{i,\ell+1} &= \sigma(\mathbf{W}_n^\ell \mathbf{h}_t^{i,\ell} + \text{MEAN}_{j \in \mathcal{N}_k(i)} \{\alpha_t^{j \rightarrow i, \ell} \mathbf{m}_t^{j \rightarrow i, \ell}\}) \end{aligned} \quad (26)$$

where $\mathbf{W}_m \in \mathbb{R}^{d_\ell \times (2d_\ell+1)}$, \mathbf{b}_m^ℓ , $\mathbf{W}_e \in \mathbb{R}^{1 \times d_\ell}$, \mathbf{b}_e^ℓ , $\mathbf{W}_n \in \mathbb{R}^{d_{\ell+1} \times d_\ell}$ are learnable parameters, and $\mathcal{N}_k(i)$ denotes the k -th order neighbors of node i in the graph. When the optional adjacency-based graph is activated, an additional diffusion convolution operator (Li et al., 2017) is further considered:

$$\mathbf{h}_t^{i,\ell+1} = \psi^\ell \left(\mathbf{h}_t^{i,\ell}, \text{AGGR}_{j \in \mathcal{N}(i)} \{\rho^\ell(\mathbf{h}_t^{i,\ell}, \mathbf{h}_t^{j,\ell}, e^{i \leftarrow j})\} \right) = \sigma(\tilde{e}_k^{i \leftarrow j} \mathbf{h}_t^{j,\ell} \Theta_{1,k}^\ell + \mathbf{h}_t^{i,\ell} \Theta_2^\ell), \quad (27)$$

where $\tilde{e}_k^{i \leftarrow j}$ is the normalized edge weight for the k -th hop, $\Theta_{1,k}^\ell, \Theta_2^\ell$ are learnable parameters.

Dense Feedforward Layer After the temporal and spatial processing, we employ a series of dense feedforward layers to increase the model capacity. Specifically, we adopt a series of residual MLP:

$$\mathbf{h}_t^{i,\ell+1} = \sigma(\mathbf{W}_r^\ell \mathbf{h}_t^{i,\ell} + \mathbf{b}_r^\ell) + \mathbf{h}_t^{i,\ell}. \quad (28)$$

MLP-based Multistep Output Layer Finally, we directly generate the multistep forecast results by using a shared MLP readout layer. $\forall h \in \{1, \dots, H\}$, we have:

$$\hat{x}_{t+h}^i = \text{MLP}(\mathbf{h}_t^{i,(L)}, \mathbf{U}_{t:t+h}, \mathbf{v}_{\phi_i}), \quad \forall i \in \{1, \dots, \bar{N}\}. \quad (29)$$

4.3. End-to-End Transferable Predictor by Inductive Learning

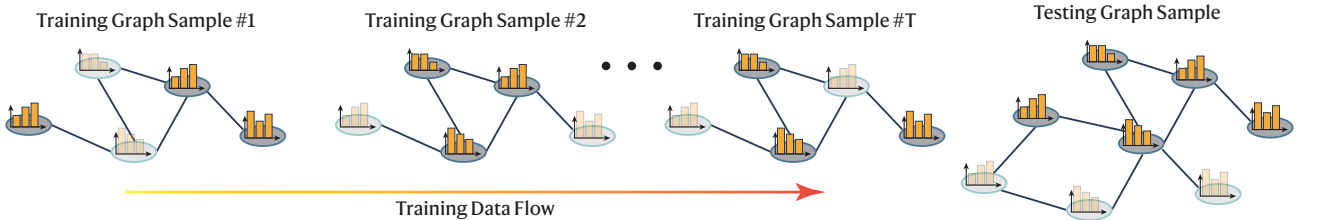


Figure 4: The inductive training scheme. During training stage, the observed regions are processed as subgraphs and are randomly masked for reconstruction purposes. During testing stage, the new regions are incorporated according to the prescribed graph structure and locations.

Using the model defined above, a straightforward solution consists of adopting an estimation model to first estimate the demand for unobserved regions and then performing downstream forecasting processing. However, we argue that the future dynamics of demand evolution in existing regions (or depots) can be substantially influenced by the newly developed regions, showing a synchronous effect for their individual demand behaviors. Therefore, we propose bypassing the estimation step and considering the forecasting backbone that can directly handle irregularly structured graph data. We aim to jointly estimate demand of newly developed regions and predict the future demand values of already existing regions in an end-to-end way, benefiting from the optimization of the shared target.

This can be modeled as an inductive learning task (Wu et al., 2021a,c; Nie et al., 2023b) associated with a *kriging* problem (Appleby et al., 2020; Lei et al., 2022; Nie et al., 2023a). We first introduce an indicating variable $\mathbf{m}_{t:t+T}^i \in \{0, 1\}^T$ to denote whether the region i has records or is masked for training purposes. The inductive training scheme constructs a random masking and reconstruction task using the observed data. We then consider

the following conditional probability during training:

$$p(\mathbf{m}_{t:t+T}^i | \mathbf{M}_{t:t+T}) = p(\mathbf{m}_{t:t+T}^i) = \mathcal{B}(\beta), \forall i \in \{1, \dots, N\}, t \in \{1, \dots, T\}, \quad (30)$$

where p is in fact a random missing probability followed a Bernoulli distribution with the parameter β (Yi et al., 2016). Notably, the existence probability of node i is independent of other nodes. Since during the model training, the location and distribution of new regions in the testing stage is unknown for the model. Thus, we do not make any assumptions on the distributions of new regions. In fact, the model should adapt to this distribution shift. For example, in the inference stage, the conditional distribution of new regions can be:

$$p(\mathbf{m}_{t:t+T}^i | \{\mathbf{m}_{t:t+T}^j\}_{j \in \mathcal{N}(i)}) \neq p(\mathbf{m}_{t:t+T}^i), \quad (31)$$

which indicates that the observed probability of region i dependents on its neighborhood regions. This is intuitive in urban logistics system. For instance, the newly developed business regions can happen within a nearby region and be influenced by each other.

Based on above discussions, the model needs to address the forecasting problem with irregular graph structures, i.e., the testing graph and node locations can differ from the ones in training. We approach this by applying the masking-reconstruction scheme proposed in (Wu et al., 2021a). As illustrated in Fig. 4, this process includes random masking and reconstruction during the training stage. Consider that we can split the training data into context-target window pairs along the temporal dimension, the following scheme is established. $\forall t \in \{1, \dots, T_{\text{train}}\}$, we have:

Sampling: $\mathbf{m}_{t-W:t}^i \sim p(\mathbf{m}_{t-W:t}^i) = \mathcal{B}(\beta), \forall i \in \{1, \dots, N_o\}$,

Masking: $\bar{\mathcal{X}}_{t-W:t} = \{\mathbf{m}_{t-W:t}^i \odot \mathbf{X}_{t-W:t}^i\}_{i=1}^{N_o}$,

Reconstructing: $\hat{\mathcal{X}}_{t:t+H} = \mathcal{F}(\bar{\mathcal{X}}_{t-W:t}, \{\mathbf{A}_\tau\}_{t-W}^t | \boldsymbol{\theta}) \approx \mathbb{E}_p[p_{\boldsymbol{\theta}}(\mathbf{x}_{t+h}^i | \bar{\mathcal{X}}_{t-W:t})], \forall h \in [1, H]$

Learning: $\boldsymbol{\theta}^* = \arg \min_{\boldsymbol{\theta}} \mathcal{L}_{\text{recon}}(\hat{\mathcal{X}}_{t-W:t}, \mathcal{X}_{t-W:t}) + \mathcal{L}_{\text{pred}}(\hat{\mathcal{X}}_{t:t+H}, \mathcal{X}_{t:t+H})$

$$= \arg \min_{\boldsymbol{\theta}} \underbrace{\sum_{\tau=t-W}^t \frac{\sum_{i=1}^{N_o} \bar{m}_\tau^i \cdot \ell(\hat{\mathbf{x}}_\tau^i, \mathbf{x}_\tau^i)}{\sum_{i=1}^{N_o} \bar{m}_\tau^i}}_{\text{reconstruction loss}} + \underbrace{\frac{1}{NH} \sum_{h=1}^H \sum_{i=1}^N \ell(\hat{\mathbf{x}}_{t+h}^i, \mathbf{x}_{t+h}^i)}_{\text{prediction loss}}, \quad (32)$$

Estimating: $\hat{\mathcal{X}}_{t:t+H'} = \mathcal{F}(\bar{\mathcal{X}}_{t-W':t}, \{\bar{\mathbf{A}}_\tau\}_{t-W'}^t | \boldsymbol{\theta}^*), \bar{\mathcal{X}}_{t-W':t} = \{\mathbf{X}_{t-W':t}^i\}_{i=1}^{N_o} \cup \{\bar{\mathbf{X}}_{t-W':t}^i\}_{i=1}^{N_u}$.

where W is the window size, H is the forecasting horizon, $\ell(\cdot)$ is some metrics such as the ℓ_1 norm and mean square error, \bar{m}_t^i is the logical binary complement of m_t^i , \mathcal{L} is the inductive training loss function, and the static covariates are omitted for ease of presentation. \mathcal{L} contains two parts: (1) the reconstruction loss in the historical window to estimate historical demand values by exploiting $\mathcal{D}_{\text{inter}}^{o,u}$; (2) the forecast loss in the future horizon to predict future demands by exploiting $\mathcal{D}_{\text{intra}}^o$ and $\mathcal{D}_{\text{intra}}^u$.

Please note that this inductive training scheme is slightly different from the self-supervised masked training scheme used in advanced Transformer-based architectures (Du et al., 2022; Nie et al., 2024a; Qiu et al., 2024). The masked training strategy used in sequential models intentionally masked out some consecutive tokens or patches, aiming to learn representations that can benefit downstream tasks in an autoregressive fashion. However, the training scheme designed in this paper is directly associated with the reconstruction task, without assumptions on the missing patterns in the testing set.

Finally, the overall solution framework is summarized in algorithm 1.

5. Experiment

This section offers extensive experiments and in-depth discussions to evaluate the proposed model. We first collect and process two real-world demand datasets, including package delivery data in China and food delivery data in the US. Our model is compared with state-of-the-art baseline models in the literature, with respect to both prediction accuracy and transferability. Then, we conduct model analysis to highlight the rationality of our model. Finally, case studies provide intuitive illustrations on the prediction results and explanations of LLM-based encodings.

5.1. Dataset Description

Two real-world logistics datasets are adopted in this study, including a package delivery dataset from (Wu et al., 2023), and a collected food delivery order datasets: (1) **Package delivery** (Wu et al., 2023): this data is

Algorithm 1: IMPEL - Overall solution framework.

Require: Partially observed lookback demand series $\mathcal{X}_{t-W:t} \in \mathbb{R}^{N_o \times d_x \times T}$; input length W ; prediction horizon H ; total number of ROIs with $\bar{N} = N_o + N_u$; coordinates of all ROIs $\bar{\mathbf{V}} \in \mathbb{R}^{\bar{N} \times d_v}$; sampling rates β , hidden dimension D ; STMP block number L ; feedforward block number L_{ffn} ; adjacency graph $\bar{\mathbf{A}} \in \mathbb{R}^{\bar{N} \times \bar{N}}$; embedding from LLMs \mathbf{H}_{LLM} ; covariates $\mathbf{U}_{t-W:t+H}$; learnable model parameters θ .

1: \triangleright Inductive model training \triangleright

2: \triangleright Masking random regions for reconstruction.

3: $\mathbf{m}_{t-W:t}^i \sim p(\mathbf{m}_{t-W:t}^i) = \mathcal{B}(\beta), \forall i \in \{1, \dots, N_o\}$, $\triangleright \mathbf{m}_{t:t+T}^i \in \{0, 1\}^T$.

4: $\bar{\mathcal{X}}_{t-W:t} = \{\mathbf{m}_{t-W:t}^i \odot \mathbf{X}_{t-W:t}^i\}_{i=1}^{N_o}$,

5: \triangleright Activate the LLM-based encoding.

6: $\mathbf{v}_{\phi_i} = \mathbf{H}_{\text{LLM}} \bar{\mathbf{W}}_{\text{prob}}, \tilde{\mathbf{v}}_{\phi_i} = \text{BATCHNORM}(\text{LEAKYRELU}(\mathbf{v}_{\phi_i}))$, $\triangleright \tilde{\mathbf{v}}_{\phi_i} \in \mathbb{R}^{D_{\text{node}}}$.

7: \triangleright Temporal encoding with LLM-based encoding using Eq. 25

8: $\mathbf{h}_t^{i,(0)} = \text{TEMPENC}([\bar{\mathcal{X}}_{t-W:t}^i \| \tilde{\mathbf{v}}_{\phi_i}], \mathbf{U}_{t-W:t}), \forall i \in \{1, \dots, N_o\}$, $\triangleright \mathbf{h}_t^{i,(0)} \in \mathbb{R}^{D_{\text{emb}}}$.

9: \triangleright Construct the LLM-based functional graph using Eq. 23.

10: $e^{i \leftrightarrow j} = \langle \mathbf{v}_{g,\phi_i}, \mathbf{v}_{g,\phi_j} \rangle, \mathcal{E} = \{e^{i \leftrightarrow j} | \forall i, j \in 1, \dots, \bar{N}\}$, \triangleright Run STMP blocks.

11: **for** ℓ in $\{1, \dots, L\}$:

12: \triangleright Graph processing using Eqs. 26 and 27 in both the adjacency and LLM-based graphs.

13: $\mathbf{h}_t^{i,(\ell+1)} = \psi^{(\ell)} \left(\mathbf{h}_t^{i,(\ell)}, \text{AGGR}_{j \in \mathcal{N}_k(i)} \{ \rho^{(\ell)}([\mathbf{h}_t^{i,(\ell)} \| \tilde{\mathbf{v}}_{\phi_i}], \mathbf{h}_t^{j,(\ell)}, a^{i \leftarrow j}, e^{i \leftrightarrow j}) \} \right)_{\ell=0}^{L-1}$, \triangleright Run MLP blocks.

14: \triangleright Dense feed-forwarding layers and the readout layer.

15: **for** ℓ in $\{1, \dots, L_{\text{mlp}}\}$:

16: $\mathbf{h}_t^{i,\ell+1} = \sigma(\mathbf{W}_r^\ell \mathbf{h}_t^{i,\ell} + \mathbf{b}_r^\ell) + \mathbf{h}_t^{i,\ell}$, \triangleright Generate predicted values.

17: $\hat{\mathbf{x}}_{t+h}^i = \text{MLP}(\mathbf{h}_t^{i,(L_{\text{mlp}})}, \mathbf{U}_{t:t+h}, \mathbf{v}_{\phi_i}), \forall i \in \{1, \dots, N_o\}, h \in \{1, \dots, H\}$, \triangleright Loss backward.

18: $\theta^* = \arg \min_{\theta} \mathcal{L}_{\text{recon}}(\hat{\mathcal{X}}_{t-W:t}, \mathcal{X}_{t-W:t}) + \mathcal{L}_{\text{pred}}(\hat{\mathcal{X}}_{t:t+H}, \mathcal{X}_{t:t+H})$,

19: **Return** Trained model $\mathcal{F}(\cdot | \theta^*)$.

20: \triangleright Inference \triangleright

21: \triangleright Given new regions with coordinates available,

22: $\hat{\mathcal{X}}_{t:t+H'} = \mathcal{F}(\bar{\mathcal{X}}_{t-W:t}, \bar{\mathbf{A}}, \bar{\mathbf{V}}, \mathbf{U} | \theta^*), \bar{\mathcal{X}}_{t-W:t} = \{\mathbf{X}_{t-W:t}^i\}_{i=1}^{N_o} \cup \{\bar{\mathbf{X}}_{t-W:t}^i\}_{i=1}^{N_u}$.

23: **Return** $\hat{\mathcal{X}}_{t:t+H'}$ \triangleright Return the prediction result.

provided by the Cainiao Network in China, containing 6 months delivery orders from five cities in China; (2) **Food delivery**: this data is provided by four different food delivery platforms in US. from 2021 to 2024. We select three representative cities with high penetration rates.

Table 2: Total number of ROIs for each city.

City	Shanghai	Hangzhou	Chongqing	Jilin	Yantai	Los Angeles	New York	San Francisco
# of ROIs	30	31	30	14	30	17	22	19

The entire area of each city is divided into several geospatial regions for logistics management. The datasets provide event-specific information, such as the order ID, pickup time, location, GPS points, courier information, delivery event, etc. Each order is attached to the corresponding region of interests (ROIs) according to its pickup GPS record. For package data, we set a time interval of 1 hour and aggregated the orders within this specified window. For food data, due to the sparsity of this data record, we select a 12-hour interval. In both datasets, we calculate the total number of pickups, i.e., the pickup demand. In following sections, we adopt both package and food delivery data for model comparisons. Individual orders are anonymized and aggregated into regions to eliminate privacy breaches. For subsequent model analysis and discussion, we mainly adopt the package delivery data for experiments. Total number of regions for each city is summarized in Tab. 2.

5.2. Experiment Settings

Evaluation scenarios. To illustrate the efficacy of our methodology, we examine three scenarios: (1) end-to-end demand joint estimation and forecasting in a single city; (2) zero-shot transfer to new cities with comprehensive observations, wherein both the source and target cities possess complete historical data; and (3) zero-shot transfer to new cities with full observations, in which both the source and target cities have newly introduced regions lacking historical data.

Baseline models. Apart from the historical average (HA) method, we select several representative models from highly related literature in machine learning studies, including: diffusion convolutional recurrent neural network (DCRNN) (Li et al., 2017), spatial-temporal convolutional neural network (Yu et al., 2017), graph wavenet (GWNET) (Wu et al., 2019b), graph learning neural network (MTGNN) (Wu et al., 2020), inductive graph neural network (IGNNK) (Wu et al., 2021b), spatial aggregation and temporal convolutional network (SATCN) (Wu et al., 2021c), message-passing gated recurrent unit (MPGRU) (Gao and Ribeiro, 2022), and graph recurrent imputation network (GRIN) (Cini et al., 2021). Particularly, DCRNN, STGCN, GWNET, MTGNN are originally designed for forecasting tasks; While IGNNK, SATCN, MPGRU, and GRIN are designed for kriging and imputation problems. We evaluate both of the two categories for a fair comparison.

Tasks setups. Models are trained to predict the future demand of all locations in the next 24 steps, given a 24-step historical window of existing regions. For Shanghai, Hangzhou, Chongqing and Yantai, we randomly choose 10 regions as newly developed regions for test. For Jilin, Los Angeles, New York and San Francisco, the number of new regions is set to 5. Note that the unknown testing regions are unavailable for all models during training and only accessible for testing purposes. Following Wu et al. (2023), we use the 6:2:2 ratio for training, evaluation and test sets based on the chronological order of the timestamps. To assess the performance of the above models, we report the metrics of Mean Absolute Error (MAE) and Root Mean Squared Error (RMSE).

Hyperparameters. For LLMs, we mainly employ an open-source model called Llama (Touvron et al., 2023). Another model called BERT (Devlin et al., 2018) is also used for comparison. For IMPEL, the LLM encoding dimension is 4096 according to the default setting of Llama. The node embedding dimension is set to 32. We totally adopt 3 layers of feedforward layers and 1 spatiotemporal message-passing layer. The hidden dimension of the sequential encoder is 64 for all data. The number of masked regions during training is set to 6 for Shanghai, Hangzhou, Chongqing, and Yantai, and 3 for others. As for hyperparameters of other baselines, we tune their parameters according to the suggested values from their original papers.

Platforms. All experiments are implemented on a single NVIDIA RTX A6000 GPU using PyTorch.

Table 3: Experimental results of spatiotemporal delivery demand joint estimation and prediction in package delivery datasets.

Models	Shanghai		Hangzhou		Chongqing		Jilin		Yantai	
	MAE	RMSE								
HA	6.96	16.41	8.94	20.56	4.00	8.85	2.27	4.85	3.82	8.42
DCRNN (Li et al., 2017)	5.65	11.86	7.33	14.59	3.53	6.15	2.05	3.37	3.21	6.17
STGCN (Yu et al., 2017)	5.07	11.62	6.38	14.26	2.99	6.00	1.53	2.84	2.80	5.79
GWNET (Wu et al., 2019b)	5.22	11.67	7.99	15.90	3.06	6.03	1.64	3.06	2.93	6.01
MTGNN (Wu et al., 2020)	5.09	11.56	6.23	13.89	2.97	5.91	1.52	2.84	2.73	5.70
IGNNK (Wu et al., 2021b)	5.22	11.50	7.25	15.06	3.22	6.06	2.22	3.71	2.97	5.93
SATCN (Wu et al., 2021c)	4.75	9.38	7.64	14.77	3.04	5.27	1.58	2.84	2.83	5.02
MPGRU (Gao and Ribeiro, 2022)	6.30	13.43	7.95	16.03	3.91	7.60	1.94	3.61	3.58	7.45
GRIN (Cini et al., 2021)	5.08	11.64	6.30	14.56	3.05	6.08	1.54	2.90	2.86	6.02
IMPEL (Ours)	3.76	7.93	4.52	9.90	2.47	4.92	1.39	2.51	2.23	4.18
Improvement (%)	20.8	15.4	27.4	28.7	16.8	6.64	8.55	11.6	18.3	16.7

5.3. Results on City-wide Demand Joint Estimation and Prediction

5.3.1. Task 1: Results of Model Comparison in Single Cities.

The results of model comparison in the two datasets are shown in Tabs. 3 and 4. As can be seen, our model consistently outperforms baselines by a large margin, especially in mega cities like Shanghai, Hangzhou, and Los Angeles. Since the joint estimation and prediction task is more challenging than the conventional time series forecasting problem, some strong baselines from the literature (such as DCRNN and GWNET) are less competitive. For models that are originally designed for imputation or kriging, i.e., GRIN and IGGNK, they are surpassed by both our model and other forecasting-based models. Surprisingly, even without complex sequential processing modules, such as RNNs and TCNs, IMPEL still achieves the best performance in all cases.

Table 4: Experimental results of spatiotemporal delivery demand joint estimation and prediction in food delivery datasets.

Models	Los Angeles		New York		San Francisco	
	MAE	RMSE	MAE	RMSE	MAE	RMSE
HA	0.602	1.157	0.792	1.400	0.438	0.766
DCRNN (Li et al., 2017)	0.481	0.983	0.602	1.132	0.328	0.644
STGCN (Yu et al., 2017)	0.466	0.903	0.569	1.050	0.297	0.623
GWNET (Wu et al., 2019b)	0.457	0.900	0.614	1.170	0.298	0.620
MTGNN (Wu et al., 2020)	0.441	0.896	0.589	1.093	0.295	0.623
IGNNK (Wu et al., 2021b)	0.448	0.907	0.573	1.062	0.301	0.616
SATCN (Wu et al., 2021c)	0.471	0.934	0.594	1.061	0.328	0.601
MPGRU (Gao and Ribeiro, 2022)	0.458	0.920	0.589	1.104	0.299	0.625
GRIN (Cini et al., 2021)	0.444	0.906	0.579	1.075	0.304	0.625
IMPEL (Ours)	0.321	0.780	0.507	0.907	0.280	0.576
Improvement (%)	27.2	12.9	10.9	13.6	5.08	4.16

Fig. 5 provides several visualization examples that are randomly chosen from the prediction results of our model. Different regions and cities show distinct demand patterns, but share some common structures such as

periodicity. Furthermore, the demand time series is sparsely sampled, with a large number of time points absent. Some data imputation methods that can be integrated in deep learning architectures can be adopted to tackle the sparse input sequence (Nie et al., 2024a).

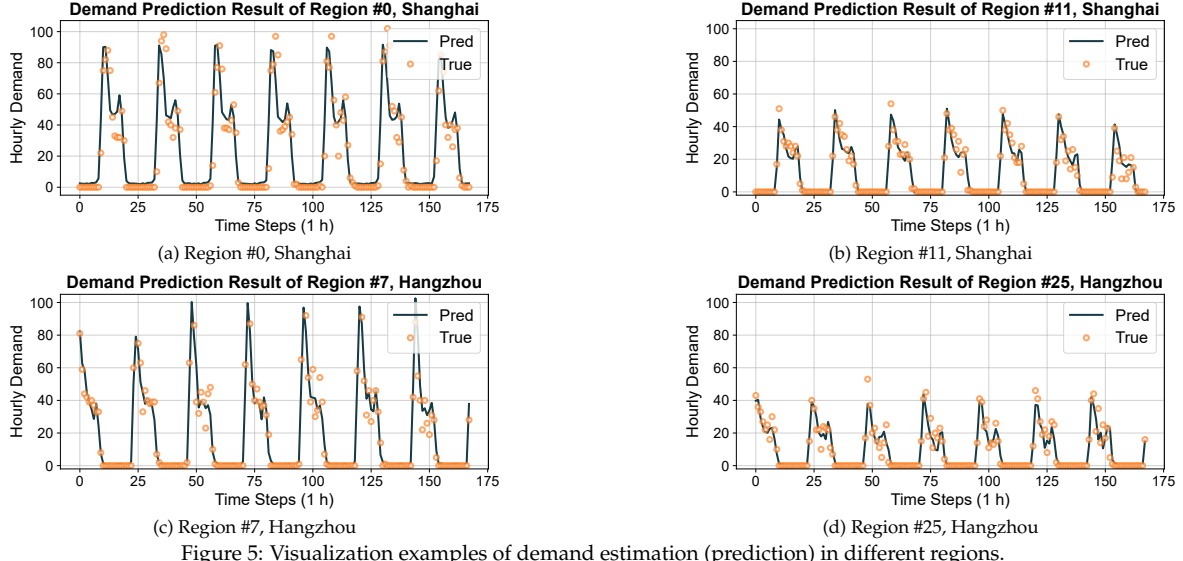


Figure 5: Visualization examples of demand estimation (prediction) in different regions.

5.3.2. Task 2: Model Transfers to New Cities with Full Observations

In addition to the accuracy of estimation and forecasting, transferability is another prominent property of the proposed model. In this section, we evaluate two aspects of model-based transfer strategy. First, we train a model on the full region sets in a source city, then we employ it to a new city with full observations, i.e., without new regions. This model needs to outputs the prediction results directly, without tuning any parameter. Second, we train and transfer models in source and target cities that both have new regions without observations.

Table 5: Experimental results of model transfer in new cities with full measurement (zero-shot prediction). We remove the spatial message passing layers in IMPEL in this case.

Models	IMPEL (Ours)		MTGNN		IGNNK		STGCN		GRIN	
	MAE	RMSE	MAE	RMSE	MAE	RMSE	MAE	RMSE	MAE	RMSE
Source \mapsto Target										
Shanghai \mapsto Hangzhou	3.35	6.42	4.07	7.32	5.64	9.00	5.55	9.31	3.75	7.33
Shanghai \mapsto Chongqing	2.26	4.44	2.62	4.89	3.25	5.22	2.91	4.91	2.51	4.86
Shanghai \mapsto Yantai	2.21	4.14	2.52	4.68	3.47	5.66	2.79	4.77	2.56	4.87
Hangzhou \mapsto Shanghai	2.90	6.20	3.12	6.38	3.04	6.26	3.09	6.54	3.11	6.53
Hangzhou \mapsto Chongqing	2.10	4.25	2.21	4.37	2.21	4.32	2.17	4.37	2.20	4.47
Hangzhou \mapsto Yantai	2.13	4.08	2.26	4.33	2.23	4.17	2.21	4.28	2.34	4.69

Tab. 5 shows the results of model transfers in the entire dataset (both the source and the target sets). This zero-shot prediction task is challenging, as different cities can have distinct demand patterns in both space and time. Through this experiment, we would like to examine whether the model learns some shared patterns of demand distribution. As demonstrated, our model shows superior transferability than other models in this pure forecasting task. Results of different source-target city pairs also indicate that different cities exhibit various demand patterns, but our model can capture the shared structures and learn to narrow this gap.

5.3.3. Task 3: Model Transfers to New Cities with New Regions

When there exist regions without historical data in both source and target domains, the challenge of model transfer is further intensified. Tab. 6 examines the performance of a mode trained in Shanghai and transferred to new cities with different numbers of new regions. As expected, the prediction error is larger than the results in Tab. 5 due to the existence of unobserved regions in both the training set and the test set. In this scenario, our model shows more significant superiority over baselines. This can be ascribed to the generality of LLM-based location encoding that has comprehensive and fundamental geospatial knowledge shared across cities.

6. Discussions

This section provides comprehensive discussions to enhance the interpretability of the proposed framework. We first discuss and interpret the role of LLM-based encodings. Then the impact of modular designs and the

Table 6: Experimental results of model transfer in new cities with partial measurement (both the source city and the target city have unobserved regions).

Source \mapsto Target	Models # of new regions	IMPEL (Ours)		MTGNN		IGNNK		STGCN	
		MAE	RMSE	MAE	RMSE	MAE	RMSE	MAE	RMSE
Shanghai \mapsto Hangzhou	5	5.33	9.26	6.51	<u>13.70</u>	6.53	13.87	7.39	14.73
	10	5.54	9.50	7.14	<u>14.29</u>	<u>7.13</u>	14.52	8.02	15.44
Shanghai \mapsto Chongqing	5	2.92	4.79	3.14	5.73	3.00	<u>5.52</u>	3.33	6.00
	10	3.09	5.02	3.45	6.16	3.35	<u>5.98</u>	3.63	6.43
Shanghai \mapsto Yantai	5	2.72	4.47	2.96	5.29	<u>2.93</u>	<u>5.19</u>	3.25	5.90
	10	2.82	4.57	<u>3.38</u>	6.26	<u>3.38</u>	<u>6.19</u>	3.68	6.80

choice of hyperparameters of analyzed. Finally, the rationality of the joint estimation and prediction is verified.

6.1. Benchmarking the LLM-based Geolocation Encoding

To justify the significance of LLM-based geolocation encoding in delivery modeling, we perform experiments to compare it with other geo-encoding methods. This section contains the following evaluations:

1. Comparison with state-of-the-art geographic embedding methods, including Space2Vec (Mai et al., 2020) and Sphere2Vec (Mai et al., 2023);
2. Encoding POIs with large embedding models, such as the General Text Embeddings (GTE) (Li et al., 2023);
3. Using one-hot encoding to process POI features;
4. Only encoding of target address with LLMs.

Table 7: Evaluation results of different geo-encoding methods.

Models	Shanghai		Hangzhou		Chongqing		Jilin		Yantai	
	MAE	RMSE								
IMPEL (Ours)	3.76	7.93	4.52	9.90	2.47	4.92	1.39	2.51	2.23	4.18
Space2Vec	4.28	7.93	5.93	10.75	6.47	10.28	1.52	2.68	3.41	6.61
Sphere2Vec	4.33	8.23	10.26	20.17	3.13	5.54	1.47	2.67	3.55	6.73
LLM+Address	5.95	14.17	4.99	10.48	2.96	5.38	1.98	4.08	2.94	5.22
POI Only	6.98	16.00	11.44	22.07	7.67	12.03	2.69	5.48	4.06	7.79
GTE+POI	4.08	8.71	5.32	11.88	3.04	5.82	1.90	4.05	2.89	4.86

Results are shown in Table 7. As can be seen, our model consistently achieves the best performances. Pretrained geographic methods such as Space2Vec cannot provide effective contextual information for delivery modeling. Additionally, encoding only the coordinates (address) or using other methods to process POIs cannot achieve desirable performances.

6.2. The generality of LLM-based Geolocation Encoding in Enhancing Demand Prediction

Recall that our model has a simple-yet-effective architecture: it bases on stacked spatiotemporal message passing layers that are easy to compute. This efficiency is achieved by the effectiveness of LLM-based encoding. To evaluate whether the enhancement of LLM-based encoding is generic, we equip other baselines with the same encoding and report their performances. The results presented in Tab. 8 indicate that all baseline architectures can benefit from the embedding, with improvements exceeding 10%. This result means that better prediction accuracy can be achieved by adopting more advanced backbone architectures.

6.3. Understanding the Encoding from LLMs

According to the discussions mentioned above, the role of LLM-based encoding is pivotal for our model. Therefore, we conduct an analysis to compare different LLM backbones and to determine whether to use the reinforcement learning from human feedback (RLHF) scheme (Bai et al., 2022). As an additional comparison, we also construct a Laplacian-based encoding that adopts the random-walk positional encoding for GNNs (Dwivedi et al., 2021), and a random encoding sampled from a Gaussian distribution (Abboud et al., 2020), which are widely used in graph machine learning studies.

There are three observations in Fig. 6. (1) Llama and BERT achieve comparable performances, showing lower error than graph-based encodings (i.e., “Laplacian” and “Random”). (2) After being processed with RLHF, the

Table 8: Performance gains by equipping with LLM-based encoding and graph.

Models	Shanghai		Hangzhou		IMP (%)
	MAE	RMSE	MAE	RMSE	
DCRNN	5.65	11.86	7.33	14.59	
+LLM Enc.	4.86	9.98	6.34	12.55	14.83%
STGCN	5.07	11.62	6.38	14.26	
+LLM Enc.	4.47	9.34	5.36	10.39	18.64%
GWNET	5.22	11.67	7.99	15.90	
+LLM Enc.	4.58	9.25	6.03	11.69	21.04%
MTGNN	5.09	11.56	6.23	13.89	
+LLM Enc.	4.05	8.15	5.45	10.38	21.92%
IGNNK	5.22	11.50	7.25	15.06	
+LLM Enc.	3.95	7.90	5.88	11.21	25.52%
SATCN	4.75	9.38	7.64	14.77	
+LLM Enc.	4.58	8.85	6.12	11.00	13.68%

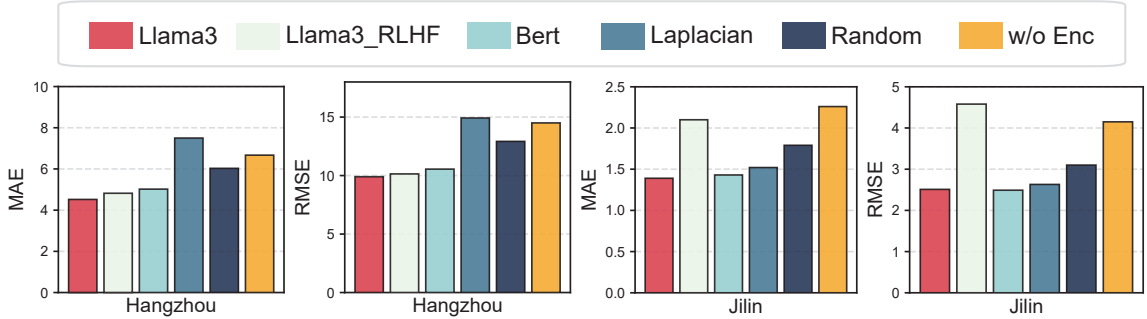


Figure 6: Ablation study on the choice of region encoding.

performance degrades a lot, which is counter-intuitive. We claim that the embedding from the output layer of LLMs tends to align with the node embedding of GNNs in the feature space. The intervention of RLHF can distort this natural alignment to some extent. (3) After removing the encoding, our model cannot achieve desirable results, which echos our collective-individual designs in section 4.2.

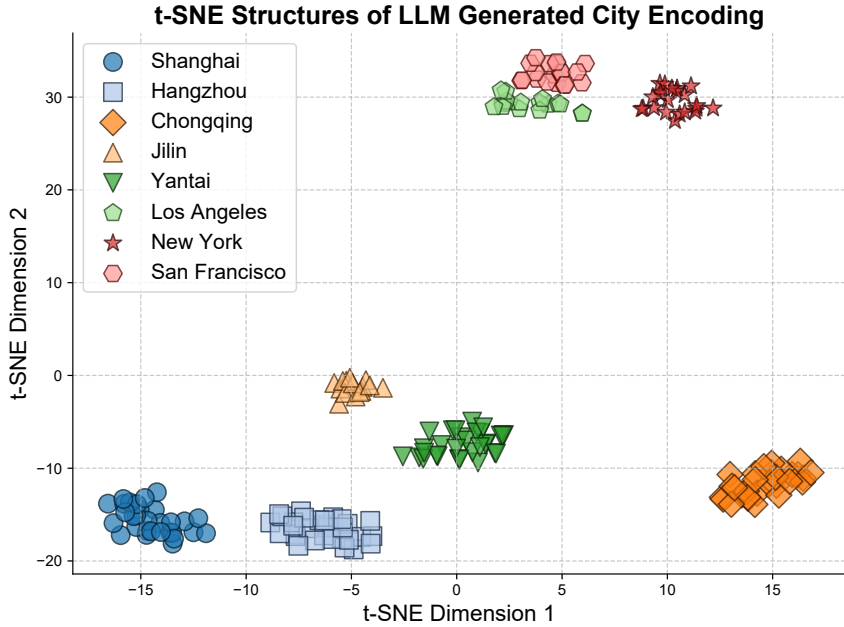


Figure 7: The t-SNE structures of LLM encoding of eight cities.

An intriguing research question pertains to the manner in which LLMs comprehend the geospatial relationship. To initiate an investigation into this matter, we present in Fig. 7 a visualization of the encoding produced by

LLMs, employing the t-SNE dimensional reduction technique. Interestingly, the encoding can differentiate different cities, and regions belonging to the same city are aggregated closely. Cities in different countries are relatively far apart, which is in line with human understanding.

6.4. Model analysis

6.4.1. Ablation Study

To justify the rationality of the integrated framework, we perform ablation study to examine the following model variations by removing or replacing existing components in IMPEL:

1. w/o LLM-graph: we remove the LLM-based graph construction and message passing layers;
2. w adjacency graph: we replace the LLM-based graph with a proximity (distance)-based graph;
3. w/o updating layers: we remove the dense feedforward layers after the message passing;
4. First update then propagate: we implement feedforward first, then message passing.

Fig. 8 displays the results of architectural ablation studies. It is apparent that the LLM-based functional graph plays a pivotal role in model performance. On the contrary, the proximity-based graph is less informative in this task. Additionally, the feedforward layers are also indispensable and can make more contributions when equipped after the message-passing layers.

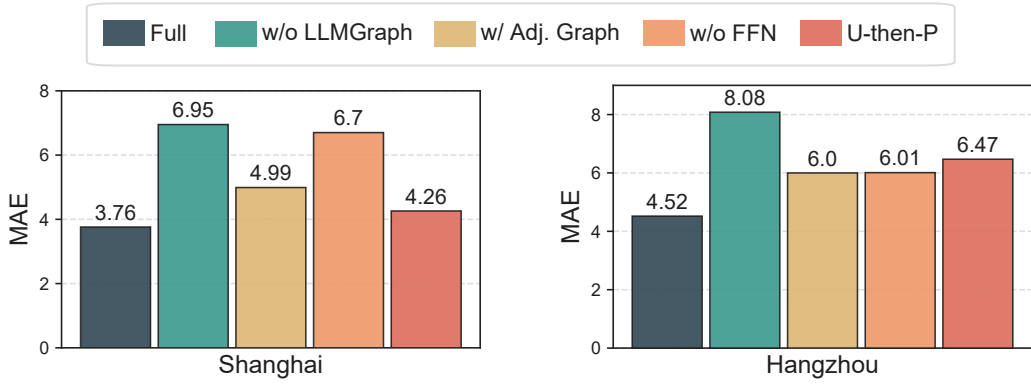


Figure 8: Ablation study on the choice of modules.

6.4.2. Sensitivity Analysis

The plot in Fig. 9 shows the influence of different observation rates, in other words, different numbers of new regions. As expected, the task becomes more challenging as more regions are developed. But our model is more robust to missing observations than the baseline IGNNK in these scenarios.

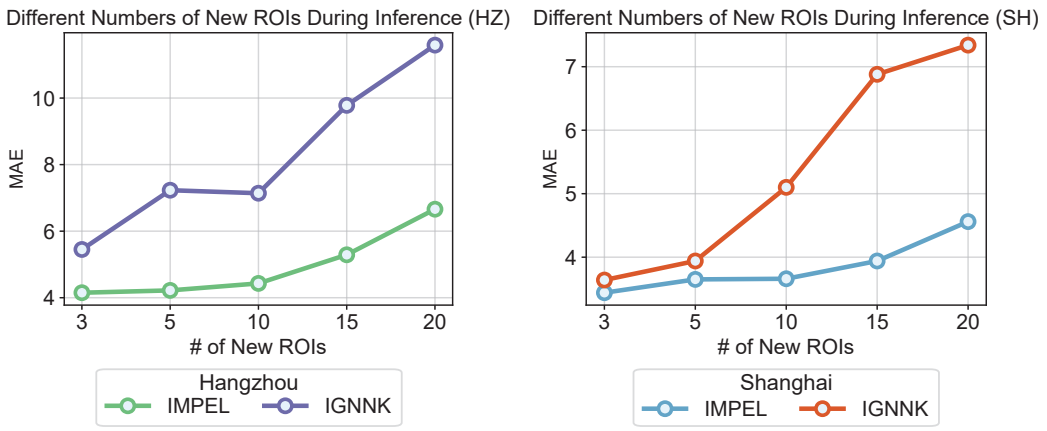


Figure 9: Model performance under different numbers of newly added regions.

In Fig. 10 we further examine the impacts of the masking strategy. Both IGNNK and IMPEL share the inductive training strategy. However, IMPEL can benefit more from the increase in masking rates during training. Even with a large proportion of regions being masked, our model can still reconstruct the target set with guaranteed accuracy, which is attributed to the versatility of LLM-encoding.

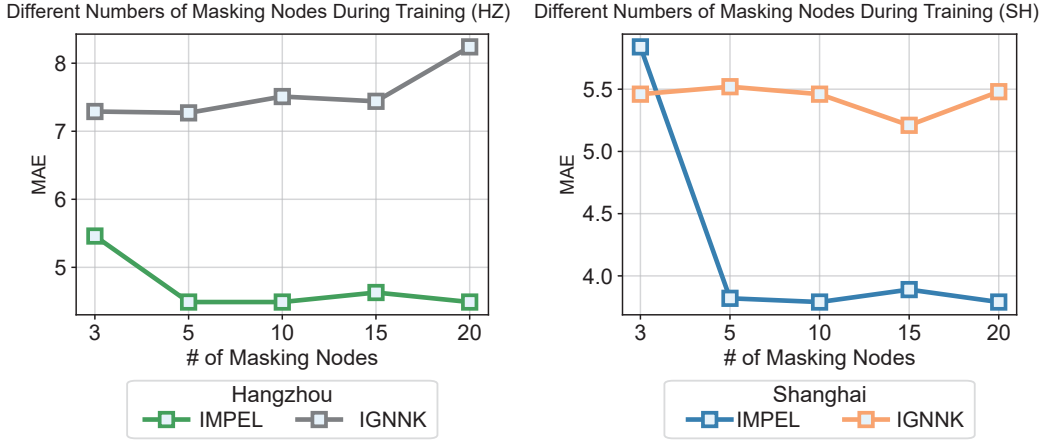


Figure 10: Model performance under different numbers of masking nodes during training.

6.4.3. Comparison with Separate Estimation and Prediction.

Furthermore, it would be beneficial to ascertain whether IMPEL enhances the kriging or forecasting capabilities. To determine this, we first train a forecasting model based on partial regions with full historical records. Then we incorporate the newly added ROIs and compare the following strategies: (1) End-to-end estimation and forecasting; (2) Direct forecasting for all regions based on the incomplete data; (3) First estimating the unknown data with a pretrained estimator, i.e., a kriging model, and then forecasting the future states of all regions. IGNNK is adopted as the pretrained kriging model; (4) First forecasting the future values of observed data, and then estimating the unobserved regions with a pretrained kriging model.

Table 9: Experimental results of model in separate estimation and forecasting tasks.

Tasks	Models	Shanghai		Hangzhou		Chongqing	
		MAE	RMSE	MAE	RMSE	MAE	RMSE
Forecasting	STGCN	3.04	6.42	3.01	5.98	2.16	4.38
	DCRNN	3.69	7.08	4.14	7.35	2.75	5.11
	GWNET	3.16	6.56	3.22	6.32	2.22	4.45
	IMPEL (Ours)	2.83	6.00	2.76	5.55	2.08	4.19
	Improvement (%)	6.91	6.54	8.31	7.19	3.70	4.34
Estimation	IGNNK	3.48	10.57	5.70	14.93	1.91	4.64
	SATCN	3.96	8.12	7.81	15.15	2.59	4.47
	IMPEL (Ours)	1.79	5.50	2.59	8.50	0.91	2.76
	Improvement (%)	48.6	32.3	54.6	43.1	52.4	38.3

As an initial evaluation, Tab. 9 report the performance of separate estimation and forecasting tasks. These models are trained on respective tasks with separate objectives. It can be seen that IMPEL has a beneficial effect on the performance of both tasks, with a particularly notable improvement in the more difficult estimation task. Tab. 10 further sheds light on the necessity of the joint estimation and prediction framework. Separate treatment can achieve a lower training error by learning to fit the full distribution. However, they over-fit the training data and generate poor generalization performance in testing set where new regions are included. Instead, our end-to-end setting balances the capacity and robustness, achieving the highest accuracy in this hybrid task.

7. Conclusion and Future Work

Accurate and real-time demand estimation and forecasting provide timely information for decision making and strategic management in urban delivery logistics. To jointly achieve the goal of estimating demand for new regions and predicting future values for existing regions, this paper introduces a graph-based deep learning framework enhanced by large language models. An inductive training scheme is then developed to promote the transfer of the model to new regions and cities. Experiments on two real-world delivery datasets, including eight cities in China and the US, show that our model significantly outperforms state-of-the-art baselines. It also has better zero-shot transferability in new cities, is more robust to the addition of new regions, and can benefit a lot from the end-to-end learning paradigm. Moreover, it is evident that the LLM-based encoding, which

Table 10: Different solution scheme and the effects of joint estimation and forecasting.

Design	Shanghai			Hangzhou		
	Training MAE	Testing MAE	Testing RMSE	Training MAE	Testing MAE	Testing RMSE
End-to-End	3.48	3.76	7.93	3.61	4.52	9.90
Direct Forecast	3.30	6.14	11.84	3.18	8.32	16.53
Estimate-then-Forecast	3.33	5.10	11.12	3.08	6.72	14.71
Forecast-then-Estimate	3.28	5.07	11.09	3.27	7.08	15.43

is geospatially aware, plays a crucial role in characterizing region-specific demand patterns and facilitating transferability across cities based on the graph constructed on it.

Although promising results have been demonstrated, there are several shortcomings need further attention. First, it is important to ensure the interpretability of the model within the logistics and delivery sector to maintain the trust of stakeholders. Our model is currently based on black-box architectures in which explainable AI techniques can be used to interpret it. Second, the estimation and transfer of demand in new regions are based on the observation of existing regions, which can lead to error accumulation.

Further research could investigate the potential of integrating this framework with more sophisticated LLM techniques, such as chain-of-thoughts prompting (Wei et al., 2022) and retrieval-augmented generation (Lewis et al., 2020), for other tasks in logistics management, including route planning and optimization, expected time of arrival estimation, and depot location optimization (Liu et al., 2023).

Acknowledgments

This research was sponsored by the National Natural Science Foundation of China (52125208), the National Natural Science Foundation of China’s Fundamental Research Program for Young Students (524B2164), and grants from the Research Grants Council of the Hong Kong Special Administrative Region, China (Project No. PolyU/15206322 and PolyU/15227424).

8. Appendix

8.1. More explanations on the role of LLM-based encoding

We provide more explanations on the role of LLM-derived embedding in the context of demand prediction and estimation. Actually, the demand prediction problem (without missing observations) can generally be considered as a time series forecasting task in which deep neural networks are applied to predict future value based on historical data. In state-of-the-art time series forecasting models, three types of additional features can be collected and used as covariates (Cini et al., 2023b): (1) time-related features, such as time-of-day and day-of-week encodings; (2) region-specific variates, such as the region (sensor) identity information and property; (3) cross-region variates, such as region-wide relationships described by an adjacency graph. These features complement the historical-future data pairs, and this setting is commonly acknowledged in previous work (Li et al., 2017; Wu et al., 2019b; Yu et al., 2017; Cini et al., 2021; Wu et al., 2020; Nie et al., 2024a).

For (1), we have performed supplementary experiments by adding timestamp features to the model in subsection 8.2.2, and the results show that the additional temporal features do not benefit the performances significantly; For (2), we use the LLM-based location encoding for each region as specialized features; For (3), we construct a functional graph based on the LLM-based encoding to quantify the relationship between regions. Therefore, the LLM-derived embedding can characterize rich information to improve prediction performance.

8.2. Supplementary experiments

8.2.1. Experiments on the observation patterns

It should be noted that the experiments described in section 5 are based on the random selection and masking of regions for evaluation purposes. This may not represent the real-world scenarios of service area expansion. To mitigate this experimental bias, we perform additional experiments that remove a whole cluster of regions that are close to each other, which leads to a cluster missing pattern. Note that the random seed is fixed for all baselines for the same city for a fair comparison. Tab. 11 provides the results on package delivery datasets. As expected, most of the baselines show worse performance due to the difficulty in model generalization. Interestingly, in some cases our model performs better than the random missing scenario and has a greater margin of improvement. This is due to the effectiveness of the LLM-based encoding for providing sufficient geolocation information about the target location.

Table 11: Experimental results of spatiotemporal delivery demand joint estimation and prediction in package delivery datasets. In these experiments, the unobserved locations are sampled not at random, i.e., a spatial cluster of regions that are near each other is removed.

Models	Shanghai		Hangzhou		Chongqing		Yantai	
	MAE	RMSE	MAE	RMSE	MAE	RMSE	MAE	RMSE
DCRNN (Li et al., 2017)	5.77	12.30	6.32	11.91	4.42	8.36	2.65	5.05
STGCN (Yu et al., 2017)	5.60	12.86	6.33	10.98	4.52	10.71	2.61	5.68
GWNET (Wu et al., 2019b)	13.06	25.21	6.32	11.43	4.52	10.24	2.72	5.73
MTGNN (Wu et al., 2020)	5.56	12.50	6.09	11.37	4.57	10.90	2.77	5.72
IGNNK (Wu et al., 2021b)	5.86	13.21	5.82	10.44	4.72	10.89	3.11	6.76
SATCN (Wu et al., 2021c)	5.06	9.31	6.57	11.15	3.64	6.62	3.37	5.78
MPGRU (Gao and Ribeiro, 2022)	6.64	14.55	7.24	13.11	5.35	11.89	3.51	7.46
GRIN (Cini et al., 2021)	5.55	12.76	5.46	10.36	4.67	11.14	2.85	6.19
IMPEL (Ours)	3.45	7.00	4.41	9.56	2.50	5.21	2.30	4.73
Improvement (%)	31.82	24.81	19.23	7.72	31.32	21.30	11.88	6.34

8.2.2. Experiments on the Temporal Modeling

A common practice in deep traffic prediction model is to process the sequence with temporal modules such as recurrent neural networks and timestamp features. Therefore, we examine the effect of temporal techniques in our architecture by equipping it with temporal modules and timestamp features. For timestamp features, we use the time-of-day and day-of-week positional encodings used in previous work (Cini et al., 2021) and concatenate them with the input time series. For additional temporal modules including RNN and TCN, we replace the original MLP in Eq. 25 with them. We report both the accuracy and training efficiency in Table 12. Performances of several baselines are also shown as a reference. It is observed that the gain of temporal modeling is marginal. However, introducing complicated temporal techniques has increased the computational burden. To this end, we choose our architecture for simplicity and better transferability.

Table 12: The impact of temporal modeling and computational efficiency (training stage) of different settings. “w/” denotes that a new module is added to the original architecture.

Models	Shanghai				Hangzhou					
	MAE	RMSE	Memory	Speed	Params.	MAE	RMSE	Memory	Speed	Params.
IMPEL (Ours)	3.76	7.93	1.5 GB	1.1 s/batch	218.6 k	4.52	9.90	1.6 GB	1.2 s/batch	218.6 k
DCRNN	5.65	11.86	2.3 GB	929.7 s/batch	2215.8 k	7.33	14.59	2.5 GB	1311.8 s/batch	2215.8 k
GWNET	5.22	11.67	3.0 GB	165.8 s/batch	2434.7 k	7.99	15.90	3.2 GB	175.0 s/batch	2435.8 k
MTGNN	5.09	11.56	1.7 GB	52.8 s/batch	2275.3 k	6.23	13.89	1.8 GB	36.9 s/batch	2338.1 k
w/ RNN	4.38	8.87	1.8 GB	8.8 s/batch	483.1 k	5.77	10.90	1.8 GB	9.2 s/batch	483.1 k
w/ TCN	4.58	8.93	1.7 GB	5.0 s/batch	376.0 k	4.89	10.75	1.8 GB	5.3 s/batch	376.0 k
w/ Time Feat.	3.76	7.93	1.5 GB	1.1 s/batch	219.8 k	4.50	9.90	1.6 GB	1.2 s/batch	219.8 k
Input 36 Steps	3.73	7.74	1.5 GB	1.1 s/batch	219.4 k	4.52	9.87	1.6 GB	1.2 s/batch	219.4 k
Input 48 Steps	3.74	7.89	1.5 GB	1.2 s/batch	220.2 k	4.55	9.95	1.6 GB	1.4 s/batch	220.2 k
Input 72 Steps	3.77	7.97	1.6 GB	1.4 s/batch	221.7 k	4.53	9.88	1.7 GB	1.4 s/batch	221.7 k

8.2.3. Online Prediction Performances and Updating Strategy

It is important to consider a real-world scenario in which data is accumulated over time. As a result, the model will likely require regular updates and maintenance in order to maintain its accuracy. We are interested in how the model will be managed and updated with new data. Accordingly, we utilize a single pretrained model derived from a limited number of observed regions and deploy it to online prediction tasks involving an increasing number of novel regions. Fig. 11 shows the online prediction results in two cities. It is noted that this figure is different from the result in Fig. 9 as only a single model is applied. Our model shows better robustness than the baseline model IGN NK in the online application stage.

Since the model is trained in an inductive manner, it can deal with increasing data scales and region numbers. The requisite accuracy can be achieved through the implementation of model fine-tuning or retraining. Additionally, the LLM-based encoding can be precalculated for all possible regions offline. This makes the online application efficient.

Regarding the online test efficiency, we evaluate the computational efficiency at both inference stage (with generated LLM-based encoding) and the LLM encoding stage. Table 13 reports the total running time and memory consumption at two different stages. It is observed that the encoding stage requires a high computational burden due to the high complexity of LLMs. Fortunately, this encoding step (a single forward pass) only needs to be

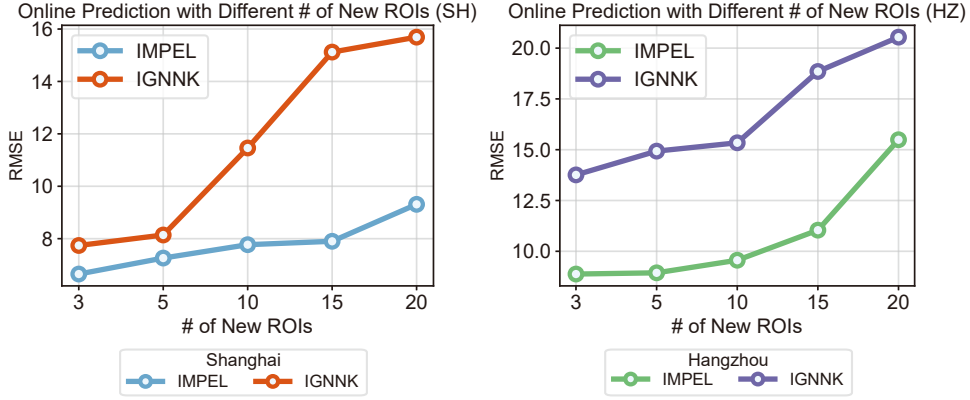


Figure 11: Online prediction performance with different numbers of newly added regions.

performed **once** throughout the testing or training phase and can also be performed **offline** after the location of the test points has been determined. After equipping the generated encoding into the prediction model, it can complete the testing task at low cost, preserving the capability of the online application.

Table 13: Computational efficiency of model inference and LLM-based encoding stages.

Models	Testing stage		LLM encoding stage		
	Running Time	GPU Memory	GPU Memory	Encoding Speed	Batch Size
IMPEL	0.17 s	1.5 GB	15.3 GB	2.48 s	1
			15.5 GB	2.04 s	4
			15.8 GB	2.11 s	8

References

Abboud, R., Ceylan, I. I., Grohe, M., Lukasiewicz, T., 2020. The surprising power of graph neural networks with random node initialization. arXiv preprint arXiv:2010.01179.

Alain, G., Bengio, Y., 2016. Understanding intermediate layers using linear classifier probes. arXiv preprint arXiv:1610.01644.

Appleby, G., Liu, L., Liu, L.-P., 2020. Kriging convolutional networks. In: Proceedings of the AAAI Conference on Artificial Intelligence. Vol. 34. pp. 3187–3194.

Azcu, I., Agatz, N., Giesen, R., 2021. Designing integrated urban delivery systems using public transport. *Transportation Research Part E: Logistics and Transportation Review* 156, 102525.

Bai, L., Yao, L., Li, C., Wang, X., Wang, C., 2020. Adaptive graph convolutional recurrent network for traffic forecasting. *Advances in neural information processing systems* 33, 17804–17815.

Bai, Y., Jones, A., Ndousse, K., Askell, A., Chen, A., DasSarma, N., Drain, D., Fort, S., Ganguli, D., Henighan, T., et al., 2022. Training a helpful and harmless assistant with reinforcement learning from human feedback. arXiv preprint arXiv:2204.05862.

Bajari, P., Nekipelov, D., Ryan, S. P., Yang, M., 2015. Machine learning methods for demand estimation. *American Economic Review* 105 (5), 481–485.

Belinkov, Y., 2022. Probing classifiers: Promises, shortcomings, and advances. *Computational Linguistics* 48 (1), 207–219.

Black, C. S., Schreffler, E. N., 2010. Understanding transport demand management and its role in delivery of sustainable urban transport. *Transportation research record* 2163 (1), 81–88.

Brown, T., Mann, B., Ryder, N., Subbiah, M., Kaplan, J. D., Dhariwal, P., Neelakantan, A., Shyam, P., Sastry, G., Askell, A., et al., 2020. Language models are few-shot learners. *Advances in neural information processing systems* 33, 1877–1901.

Chang, C., Peng, W.-C., Chen, T.-F., 2023. Llm4ts: Two-stage fine-tuning for time-series forecasting with pre-trained llms. arXiv preprint arXiv:2308.08469.

Chen, S.-A., Li, C.-L., Yoder, N., Arik, S. O., Pfister, T., 2023. Tsmixer: An all-mlp architecture for time series forecasting. arXiv preprint arXiv:2303.06053.

Cini, A., Marisca, I., Alippi, C., 2021. Filling the g_ap_s: Multivariate time series imputation by graph neural networks. arXiv preprint arXiv:2108.00298.

Cini, A., Marisca, I., Bianchi, F. M., Alippi, C., 2022. Scalable spatiotemporal graph neural networks. arXiv preprint arXiv:2209.06520.

Cini, A., Marisca, I., Zambon, D., Alippi, C., 2023a. Graph deep learning for time series forecasting. arXiv preprint arXiv:2310.15978.

Cini, A., Marisca, I., Zambon, D., Alippi, C., 2023b. Taming local effects in graph-based spatiotemporal forecasting. arXiv preprint arXiv:2302.04071.

De Felice, G., Cini, A., Zambon, D., Gusev, V. V., Alippi, C., 2024. Graph-based virtual sensing from sparse and partial multivariate observations. arXiv preprint arXiv:2402.12598.

Devlin, J., Chang, M.-W., Lee, K., Toutanova, K., 2018. Bert: Pre-training of deep bidirectional transformers for language understanding. arXiv preprint arXiv:1810.04805.

Du, W., Côté, D., Liu, Y., 2022. Saits: Self-attention-based imputation for time series. arXiv preprint arXiv:2202.08516.

Dwivedi, V. P., Luu, A. T., Laurent, T., Bengio, Y., Bresson, X., 2021. Graph neural networks with learnable structural and positional representations. arXiv preprint arXiv:2110.07875.

Fabusuyi, T., Twumasi-Boakye, R., Broaddus, A., Fishelson, J., Hampshire, R. C., 2020. Estimating small area demand for online package delivery. *Journal of Transport Geography* 88, 102864.

Fancello, G., Paddeu, D., Fadda, P., 2017. Investigating last food mile deliveries: A case study approach to identify needs of food delivery demand. *Research in transportation economics* 65, 56–66.

Gao, C., Zhang, F., Wu, G., Hu, Q., Ru, Q., Hao, J., He, R., Sun, Z., 2021. A deep learning method for route and time prediction in food delivery service. In: *Proceedings of the 27th ACM SIGKDD Conference on Knowledge Discovery & Data Mining*. pp. 2879–2889.

Gao, J., Ribeiro, B., 2022. On the equivalence between temporal and static equivariant graph representations. In: *International Conference on Machine Learning*. PMLR, pp. 7052–7076.

Garza, A., Mergenthaler-Canseco, M., 2023. Timegpt-1. arXiv preprint arXiv:2310.03589.

Gong, L., Lin, Y., Zhang, X., Lu, Y., Han, X., Liu, Y., Guo, S., Lin, Y., Wan, H., 2024. Mobility-llm: Learning visiting intentions and travel preferences from human mobility data with large language models. arXiv preprint arXiv:2411.00823.

Graffiti, R., Flunkert, V., Salinas, D., Januschowski, T., Seeger, M., Archambeau, C., 2021. Meta-forecasting by combining global deep representations with local adaptation. arXiv preprint arXiv:2111.03418.

Guo, S., Lin, Y., Feng, N., Song, C., Wan, H., 2019. Attention based spatial-temporal graph convolutional networks for traffic flow forecasting. In: *Proceedings of the AAAI Conference on Artificial Intelligence*. Vol. 33. pp. 922–929.

Gurnee, W., Tegmark, M., 2023. Language models represent space and time. arXiv preprint arXiv:2310.02207.

Haklay, M., Weber, P., 2008. Openstreetmap: User-generated street maps. *IEEE Pervasive computing* 7 (4), 12–18.

He, S., Shin, K. G., 2020. Dynamic flow distribution prediction for urban dockless e-scooter sharing reconfiguration. In: *Proceedings of the web conference 2020*. pp. 133–143.

He, X., He, F., Li, L., Zhang, L., Xiao, G., 2022. A route network planning method for urban air delivery. *Transportation Research Part E: Logistics and Transportation Review* 166, 102872.

Hess, A., Spinler, S., Winkenbach, M., 2021. Real-time demand forecasting for an urban delivery platform. *Transportation Research Part E: Logistics and Transportation Review* 145, 102147.

Isufi, E., Loukas, A., Perraudin, N., Leus, G., 2019. Forecasting time series with varma recursions on graphs. *IEEE Transactions on Signal Processing* 67 (18), 4870–4885.

Janjevic, M., Winkenbach, M., Merchán, D., 2019. Integrating collection-and-delivery points in the strategic design of urban last-mile e-commerce distribution networks. *Transportation Research Part E: Logistics and Transportation Review* 131, 37–67.

Jia, F., Wang, K., Zheng, Y., Cao, D., Liu, Y., 2024. Gpt4mts: Prompt-based large language model for multimodal time-series forecasting. In: *Proceedings of the AAAI Conference on Artificial Intelligence*. Vol. 38. pp. 23343–23351.

Jiang, A. Q., Sablayrolles, A., Mensch, A., Bamford, C., Chaplot, D. S., Casas, D. d. l., Bressand, F., Lengyel, G., Lample, G., Saulnier, L., et al., 2023. Mistral 7b. arXiv preprint arXiv:2310.06825.

Jin, M., Wang, S., Ma, L., Chu, Z., Zhang, J. Y., Shi, X., Chen, P.-Y., Liang, Y., Li, Y.-F., Pan, S., et al., 2023a. Time-llm: Time series forecasting by reprogramming large language models. arXiv preprint arXiv:2310.01728.

Jin, M., Wen, Q., Liang, Y., Zhang, C., Xue, S., Wang, X., Zhang, J., Wang, Y., Chen, H., Li, X., et al., 2023b. Large models for time series and spatio-temporal data: A survey and outlook. arXiv preprint arXiv:2310.10196.

Kojima, T., Gu, S. S., Reid, M., Matsuo, Y., Iwasawa, Y., 2022. Large language models are zero-shot reasoners. *Advances in neural information processing systems* 35, 22199–22213.

Lei, M., Labbe, A., Wu, Y., Sun, L., 2022. Bayesian kernelized matrix factorization for spatiotemporal traffic data imputation and kriging. *IEEE Transactions on Intelligent Transportation Systems* 23 (10), 18962–18974.

Lewis, P., Perez, E., Piktus, A., Petroni, F., Karpukhin, V., Goyal, N., Küttler, H., Lewis, M., Yih, W.-t., Rocktäschel, T., et al., 2020. Retrieval-augmented generation for knowledge-intensive nlp tasks. *Advances in Neural Information Processing Systems* 33, 9459–9474.

Li, X., Luo, W., Yuan, M., Wang, J., Lu, J., Wang, J., Lü, J., Zeng, J., 2021. Learning to optimize industry-scale dynamic pickup and delivery problems. In: *2021 IEEE 37th international conference on data engineering (ICDE)*. IEEE, pp. 2511–2522.

Li, Y., Yu, R., Shahabi, C., Liu, Y., 2017. Diffusion convolutional recurrent neural network: Data-driven traffic forecasting. arXiv preprint arXiv:1707.01926.

Li, Y., Yu, R., Shahabi, C., Liu, Y., 2018. Diffusion convolutional recurrent neural network: Data-driven traffic forecasting. In: International Conference on Learning Representations.

Li, Z., Xia, L., Tang, J., Xu, Y., Shi, L., Xia, L., Yin, D., Huang, C., 2024. Urbangpt: Spatio-temporal large language models. arXiv preprint arXiv:2403.00813.

Li, Z., Zhang, X., Zhang, Y., Long, D., Xie, P., Zhang, M., 2023. Towards general text embeddings with multi-stage contrastive learning. arXiv preprint arXiv:2308.03281.

Liang, J., Ke, J., Wang, H., Ye, H., Tang, J., 2023a. A poisson-based distribution learning framework for short-term prediction of food delivery demand ranges. *IEEE Transactions on Intelligent Transportation Systems*.

Liang, Y., Ding, F., Huang, G., Zhao, Z., 2023b. Deep trip generation with graph neural networks for bike sharing system expansion. *Transportation Research Part C: Emerging Technologies* 154, 104241.

Liang, Y., Huang, G., Zhao, Z., 2023c. Cross-mode knowledge adaptation for bike sharing demand prediction using domain-adversarial graph neural networks. *IEEE Transactions on Intelligent Transportation Systems*.

Liang, Y., Liu, Y., Wang, X., Zhao, Z., 2024a. Exploring large language models for human mobility prediction under public events. *Computers, Environment and Urban Systems* 112, 102153.

Liang, Y., Zhao, Z., Ding, F., Tang, Y., He, Z., 2024b. Time-dependent trip generation for bike sharing planning: A multi-task memory-augmented graph neural network. *Information Fusion* 106, 102294.

Liang, Y., Zhao, Z., Sun, L., 2022. Memory-augmented dynamic graph convolution networks for traffic data imputation with diverse missing patterns. *Transportation Research Part C: Emerging Technologies* 143, 103826.

Liang, Y., Zhao, Z., Webster, C., 2024c. Generating sparse origin–destination flows on shared mobility networks using probabilistic graph neural networks. *Sustainable Cities and Society* 114, 105777.

Liu, Y., Wu, F., Liu, Z., Wang, K., Wang, F., Qu, X., 2023. Can language models be used for real-world urban-delivery route optimization? *The Innovation* 4 (6).

Mai, G., Janowicz, K., Yan, B., Zhu, R., Cai, L., Lao, N., 2020. Multi-scale representation learning for spatial feature distributions using grid cells. arXiv preprint arXiv:2003.00824.

Mai, G., Xuan, Y., Zuo, W., He, Y., Song, J., Ermon, S., Janowicz, K., Lao, N., 2023. Sphere2vec: A general-purpose location representation learning over a spherical surface for large-scale geospatial predictions. *ISPRS Journal of Photogrammetry and Remote Sensing* 202, 439–462.

Manvi, R., Khanna, S., Burke, M., Lobell, D., Ermon, S., 2024. Large language models are geographically biased. arXiv preprint arXiv:2402.02680.

Manvi, R., Khanna, S., Mai, G., Burke, M., Lobell, D., Ermon, S., 2023. Geollm: Extracting geospatial knowledge from large language models. arXiv preprint arXiv:2310.06213.

Marisca, I., Cini, A., Alippi, C., 2022. Learning to reconstruct missing data from spatiotemporal graphs with sparse observations. arXiv preprint arXiv:2205.13479.

Muñozuri, J., Cortés, P., Onieva, L., Guadix, J., 2012. Estimation of daily vehicle flows for urban freight deliveries. *Journal of urban planning and development* 138 (1), 43–52.

Nie, T., Qin, G., Ma, W., Mei, Y., Sun, J., 2024a. Imputefomer: Low rankness-induced transformers for generalizable spatiotemporal imputation. In: Proceedings of the 30th ACM SIGKDD Conference on Knowledge Discovery and Data Mining. pp. 2260–2271.

Nie, T., Qin, G., Ma, W., Sun, J., 2024b. Spatiotemporal implicit neural representation as a generalized traffic data learner. *Transportation Research Part C: Emerging Technologies* 169, 104890.

Nie, T., Qin, G., Sun, L., Ma, W., Mei, Y., Sun, J., 2024c. Contextualizing mlp-mixers spatiotemporally for urban traffic data forecast at scale. *IEEE Transactions on Intelligent Transportation Systems*.

Nie, T., Qin, G., Wang, Y., Sun, J., 2023a. Correlating sparse sensing for large-scale traffic speed estimation: A laplacian-enhanced low-rank tensor kriging approach. *Transportation Research Part C: Emerging Technologies* 152, 104190.

Nie, T., Qin, G., Wang, Y., Sun, J., 2023b. Towards better traffic volume estimation: Jointly addressing the underdetermination and nonequilibrium problems with correlation-adaptive gnns. *Transportation Research Part C: Emerging Technologies* 157, 104402.

Nie, Y., Nguyen, N. H., Sinthong, P., Kalagnanam, J., 2022. A time series is worth 64 words: Long-term forecasting with transformers. arXiv preprint arXiv:2211.14730.

Nuzzolo, A., Comi, A., 2014. Urban freight demand forecasting: a mixed quantity/delivery/vehicle-based model. *Transportation Research Part E: Logistics and Transportation Review* 65, 84–98.

Qiu, S., Qin, G., Wong, M., Sun, J., 2024. Routesformer: A sequence-based route choice transformer for efficient path inference from sparse trajectories. *Transportation Research Part C: Emerging Technologies* 162, 104552.

Qu, X., Lin, H., Liu, Y., 2023. Envisioning the future of transportation: Inspiration of chatgpt and large models. *Communications in Transportation Research* 3.

Reed, S., Campbell, A. M., Thomas, B. W., 2024. Does parking matter? the impact of parking time on last-mile delivery optimization. *Transportation Research Part E: Logistics and Transportation Review* 181, 103391.

Satorras, V. G., Rangapuram, S. S., Januschowski, T., 2022. Multivariate time series forecasting with latent graph inference. arXiv preprint arXiv:2203.03423.

Shao, Z., Zhang, Z., Wang, F., Wei, W., Xu, Y., 2022a. Spatial-temporal identity: A simple yet effective baseline for multivariate time series forecasting. In: Proceedings of the 31st ACM International Conference on Information & Knowledge Management. pp. 4454–4458.

Shao, Z., Zhang, Z., Wang, F., Wei, W., Xu, Y., 2022b. Spatial-temporal identity: A simple yet effective baseline for multivariate time series forecasting. In: Proceedings of the 31st ACM International Conference on Information & Knowledge Management. pp. 4454–4458.

Shao, Z., Zhang, Z., Wei, W., Wang, F., Xu, Y., Cao, X., Jensen, C. S., 2022c. Decoupled dynamic spatial-temporal graph neural network for traffic forecasting. arXiv preprint arXiv:2206.09112.

Srinivas, S., Ramachandiran, S., Rajendran, S., 2022. Autonomous robot-driven deliveries: A review of recent developments and future directions. *Transportation research part E: logistics and transportation review* 165, 102834.

Suguna, M., Shah, B., Raj, S. K., Suresh, M., 2021. A study on the influential factors of the last mile delivery projects during covid-19 era. *Operations Management Research*, 1–14.

Tang, Y., Wang, Z., Qu, A., Yan, Y., Hou, K., Zhuang, D., Guo, X., Zhao, J., Zhao, Z., Ma, W., 2024. Synergizing spatial optimization with large language models for open-domain urban itinerary planning. arXiv preprint arXiv:2402.07204.

Touvron, H., Lavril, T., Izacard, G., Martinet, X., Lachaux, M.-A., Lacroix, T., Rozière, B., Goyal, N., Hambro, E., Azhar, F., et al., 2023. Llama: Open and efficient foundation language models. arXiv preprint arXiv:2302.13971.

Wang, J., Jiang, R., Yang, C., Wu, Z., Onizuka, M., Shibusaki, R., Koshizuka, N., Xiao, C., 2024. Large language models as urban residents: An llm agent framework for personal mobility generation. arXiv preprint arXiv:2402.14744.

Wang, X., Fang, M., Zeng, Z., Cheng, T., 2023. Where would i go next? large language models as human mobility predictors. arXiv preprint arXiv:2308.15197.

Wei, J., Bosma, M., Zhao, V. Y., Guu, K., Yu, A. W., Lester, B., Du, N., Dai, A. M., Le, Q. V., 2021. Finetuned language models are zero-shot learners. arXiv preprint arXiv:2109.01652.

Wei, J., Wang, X., Schuurmans, D., Bosma, M., Xia, F., Chi, E., Le, Q. V., Zhou, D., et al., 2022. Chain-of-thought prompting elicits reasoning in large language models. *Advances in neural information processing systems* 35, 24824–24837.

Wei, T., Lin, Y., Guo, S., Lin, Y., Zhao, Y., Jin, X., Wu, Z., Wan, H., 2024. Inductive and adaptive graph convolution networks equipped with constraint task for spatial-temporal traffic data kriging. *Knowledge-Based Systems* 284, 111325.

Wen, H., Lin, Y., Mao, X., Wu, F., Zhao, Y., Wang, H., Zheng, J., Wu, L., Hu, H., Wan, H., 2022. Graph2route: A dynamic spatial-temporal graph neural network for pick-up and delivery route prediction. In: Proceedings of the 28th ACM SIGKDD conference on knowledge discovery and data mining. pp. 4143–4152.

Wen, H., Lin, Y., Wu, L., Mao, X., Cai, T., Hou, Y., Guo, S., Liang, Y., Jin, G., Zhao, Y., et al., 2024. A survey on service route and time prediction in instant delivery: Taxonomy, progress, and prospects. *IEEE Transactions on Knowledge and Data Engineering*.

Wu, F., Wu, L., 2019. Deepeta: a spatial-temporal sequential neural network model for estimating time of arrival in package delivery system. In: Proceedings of the AAAI conference on artificial intelligence. Vol. 33. pp. 774–781.

Wu, L., Wen, H., Hu, H., Mao, X., Xia, Y., Shan, E., Zhen, J., Lou, J., Liang, Y., Yang, L., et al., 2023. Lade: The first comprehensive last-mile delivery dataset from industry. arXiv preprint arXiv:2306.10675.

Wu, Y., Zhuang, D., Labbe, A., Sun, L., 2021a. Inductive graph neural networks for spatiotemporal kriging. In: Proceedings of the AAAI Conference on Artificial Intelligence. Vol. 35. pp. 4478–4485.

Wu, Y., Zhuang, D., Labbe, A., Sun, L., 2021b. Inductive graph neural networks for spatiotemporal kriging. In: Proceedings of the AAAI Conference on Artificial Intelligence. Vol. 35. pp. 4478–4485.

Wu, Y., Zhuang, D., Lei, M., Labbe, A., Sun, L., 2021c. Spatial aggregation and temporal convolution networks for real-time kriging. arXiv preprint arXiv:2109.12144.

Wu, Z., Pan, S., Long, G., Jiang, J., Chang, X., Zhang, C., 2020. Connecting the dots: Multivariate time series forecasting with graph neural networks. In: Proceedings of the 26th ACM SIGKDD international conference on knowledge discovery & data mining. pp. 753–763.

Wu, Z., Pan, S., Long, G., Jiang, J., Zhang, C., 2019a. Graph wavenet for deep spatial-temporal graph modeling. In: Proceedings of the 28th International Joint Conference on Artificial Intelligence. pp. 1907–1913.

Wu, Z., Pan, S., Long, G., Jiang, J., Zhang, C., 2019b. Graph wavenet for deep spatial-temporal graph modeling. arXiv preprint arXiv:1906.00121.

Xue, J., Ka, E., Feng, Y., Ukkusuri, S. V., 2024. Network macroscopic fundamental diagram-informed graph learning for traffic state imputation. *Transportation Research Part B: Methodological*, 102996.

Xue, J., Tan, R., Ma, J., Ukkusuri, S. V., 2025. Data mining in transportation networks with graph neural networks: A review and outlook. arXiv preprint arXiv:2501.16656.

Yannis, G., Golias, J., Antoniou, C., 2006. Effects of urban delivery restrictions on traffic movements. *Transportation Planning and Technology* 29 (4), 295–311.

Yao, X., Gao, Y., Zhu, D., Manley, E., Wang, J., Liu, Y., 2020. Spatial origin-destination flow imputation using graph convolutional networks. *IEEE Transactions on Intelligent Transportation Systems* 22 (12), 7474–7484.

Yi, X., Zheng, Y., Zhang, J., Li, T., 2016. St-mvl: Filling missing values in geo-sensory time series data. In: Proceedings of the 25th international joint conference on artificial intelligence.

Yu, B., Yin, H., Zhu, Z., 2017. Spatio-temporal graph convolutional networks: A deep learning framework for traffic forecasting. arXiv preprint arXiv:1709.04875.

Yu, B., Yin, H., Zhu, Z., 2018. Spatio-temporal graph convolutional networks: a deep learning framework for traffic forecasting. In: Proceedings of the 27th International Joint Conference on Artificial Intelligence. pp. 3634–3640.

Zeng, Y., Tong, Y., Chen, L., 2019. Last-mile delivery made practical: An efficient route planning framework with theoretical guarantees. Proceedings of the VLDB Endowment 13 (3), 320–333.

Zhang, K., Zhou, F., Wu, L., Xie, N., He, Z., 2024a. Semantic understanding and prompt engineering for large-scale traffic data imputation. Information Fusion 102, 102038.

Zhang, S., Li, T., Hui, S., Li, G., Liang, Y., Yu, L., Jin, D., Li, Y., 2023. Deep transfer learning for city-scale cellular traffic generation through urban knowledge graph. In: Proceedings of the 29th ACM SIGKDD Conference on Knowledge Discovery and Data Mining. pp. 4842–4851.

Zhang, Z., Sun, Y., Wang, Z., Nie, Y., Ma, X., Sun, P., Li, R., 2024b. Large language models for mobility in transportation systems: A survey on forecasting tasks. arXiv preprint arXiv:2405.02357.

Zheng, C., Fan, X., Wang, C., Qi, J., 2020. Gman: A graph multi-attention network for traffic prediction. In: Proceedings of the AAAI Conference on Artificial Intelligence. Vol. 34. pp. 1234–1241.

Zheng, C., Fan, X., Wang, C., Qi, J., Chen, C., Chen, L., 2023. Increase: Inductive graph representation learning for spatio-temporal kriging. In: Proceedings of the ACM Web Conference 2023. pp. 673–683.